Supplementary Information for:

Anion specificity induced conformational changes in cresol-based tripodal podands controlled by weak interactions: Structural and Hirshfeld surface analysis

*Sandeep Kumar Dey, Avijit Pramanik and Gopal Das**

Department of Chemistry, Indian Institute of Technology Guwahati, Assam-781039, India

E-mail: gdas@iitg.ernet.in

Experimental Section

Competitive crystallization experiments

In a representative competitive crystallization experiments, $\mathbf{L_{1-3}}$ was placed in a beaker and dissolved in methanol (25 mg in 10 mL). For an experiment with perchlorate, 10 systems were prepared for each ligand. Solutions of $(NH_4^{+})_aX$ or NaX (X = Cl^-, Br^-, I^-, AcO^-, BO_3^{3-}, CO_3^{2-}, NO_3^-, SO_4^{2-}, PO_4^{3-}, BF_4^-; *a* = number of cations to balance the negative charge) was added to the ligand solution in the molar ratio of 1:1 (competitive anion:**L**). Then, $HClO_4$ was added to the reaction mixtures in the molar ratio of 1:1 ($HClO_4$:**L**), the beakers were covered with aluminium foil and left for few days for crystallisation to occur. The obtained crystalline material (morphologically identical) was filtered off and dried. The products were characterized by infrared spectroscopy (perchlorate showed characteristic peaks in IR spectra) and melting point measurements. The near quantitative formation of complex **1**, **2** and **3** were observed in all cases except in the cases of spherical halide anions.

Table S1. Yield of complexes **1, 2** and **3** in presence of various competing anions in 1**:**1 ratio.

Competitive Anion	$HClO_4$ **:** $\mathbf{L}_1$ (1**:**1)	$HClO_4$ **:** $\mathbf{L}_2$ (1**:**1)	$HClO_4$ **:** $\mathbf{L}_3$ (1**:**1)
	Yield of **1** (%)	Yield of **2** (%)	Yield of **3** (%)
Cl^-	54	46	38
Br^-	51	41	32
I^-	58	45	35
AcO^-	92	91	91
BO_3^{3-}	90	90	88
CO_3^{2-}	92	87	88
NO_3^-	82	80	78
SO_4^{2-}	84	81	76
PO_4^{3-}	87	84	85
BF_4^-	91	88	90
	1**:**1	1**:**1	1**:**1
	Competitive anion **:** ClO_4^-	Competitive anion **:** ClO_4^-	Competitive anion **:** ClO_4^-

Characterization of ligands.

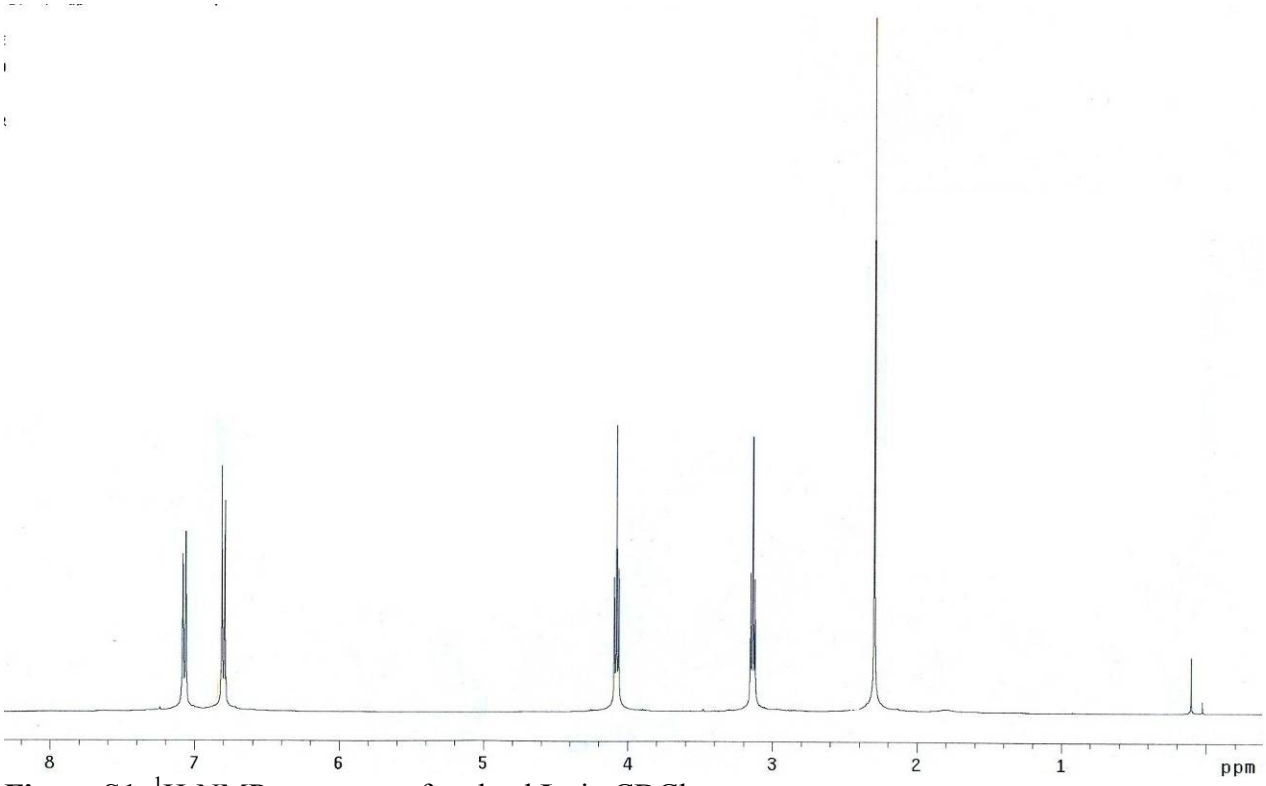

Figure S1. ^{1}H-NMR spectrum of podand $\mathbf{L_1}$ in $CDCl_3$.

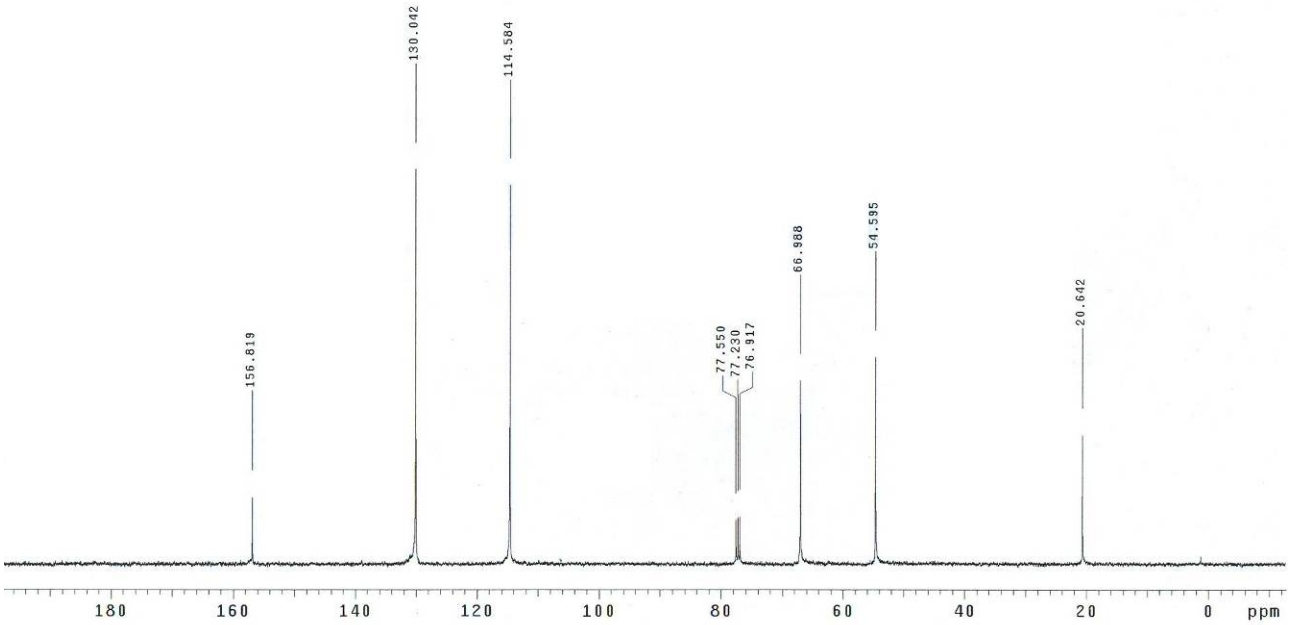

Figure S2. ^{13}C-NMR spectrum of podand $\mathbf{L_1}$ in $CDCl_3$.

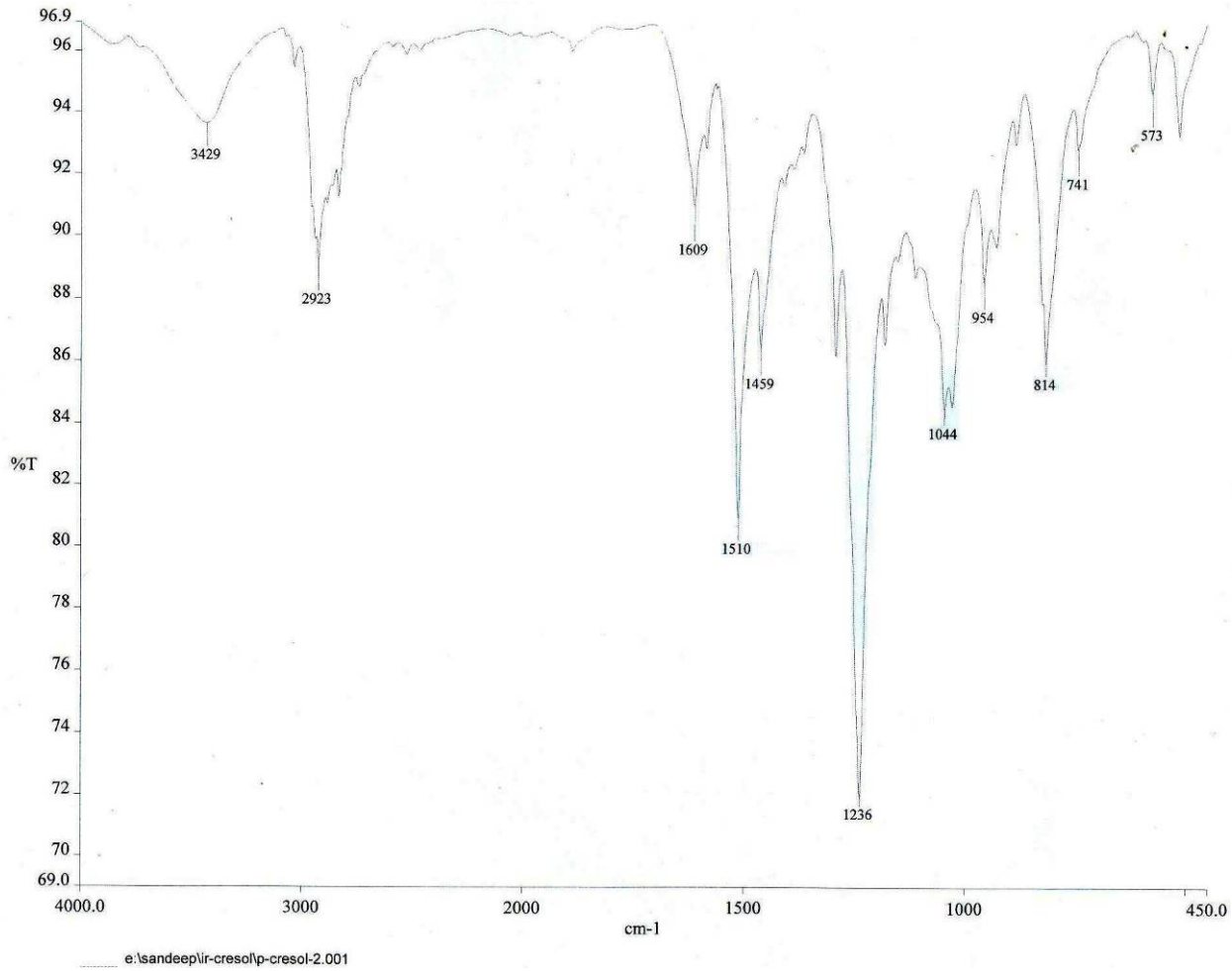

Figure S3. FT-IR spectrum of podand $\mathbf{L_1}$ (KBr pellet).

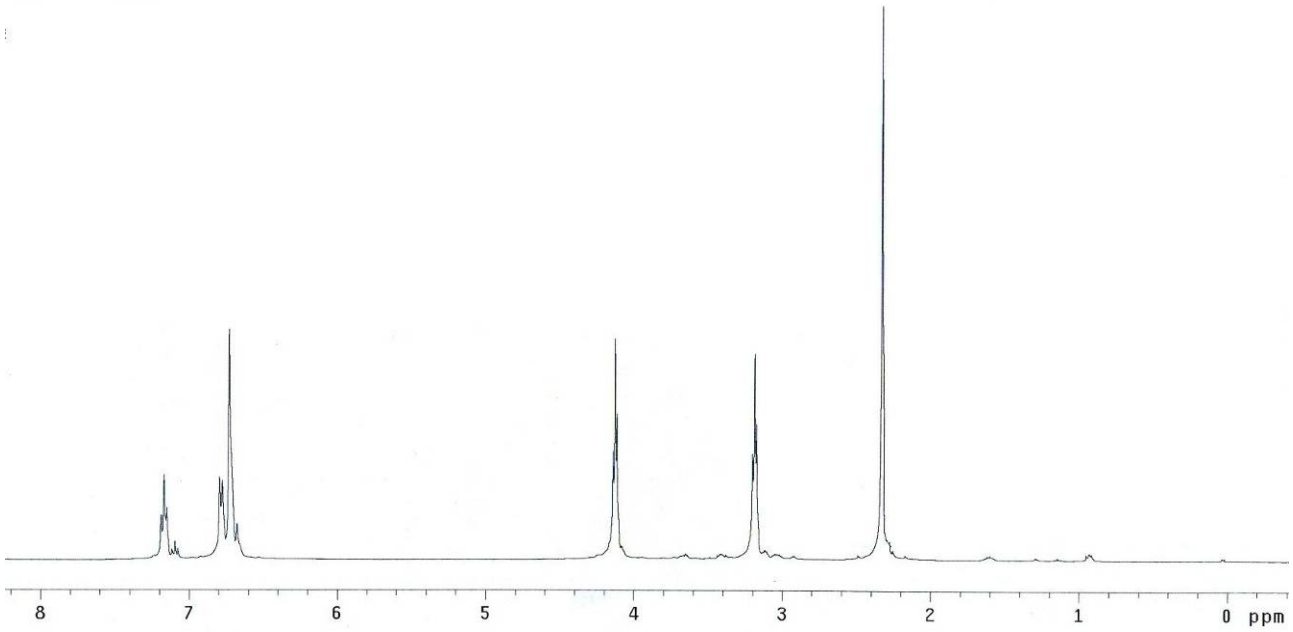

Figure S4. ^{1}H-NMR spectrum of podand $\mathbf{L_2}$ in $CDCl_3$.

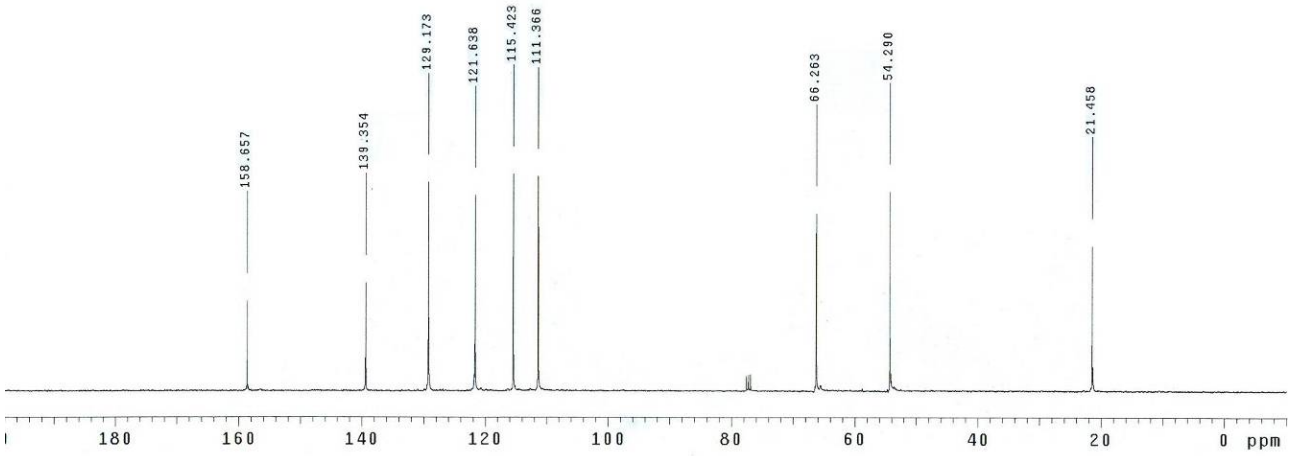

Figure S5. ^{13}C-NMR spectrum of podand $\mathbf{L_2}$ in $CDCl_3$.

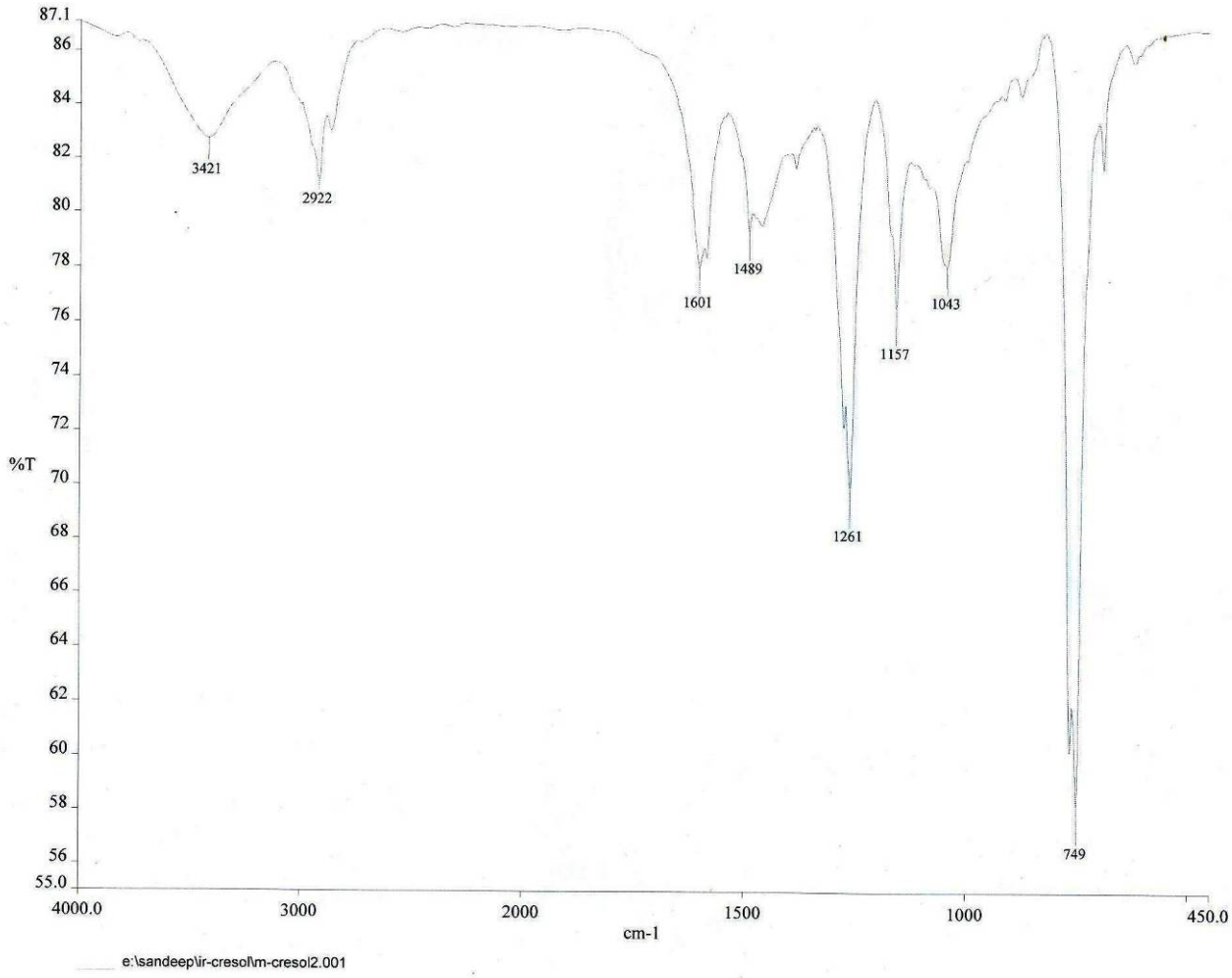

Figure S6. FT-IR spectrum of podand $\mathbf{L_2}$ (KBr pellet).

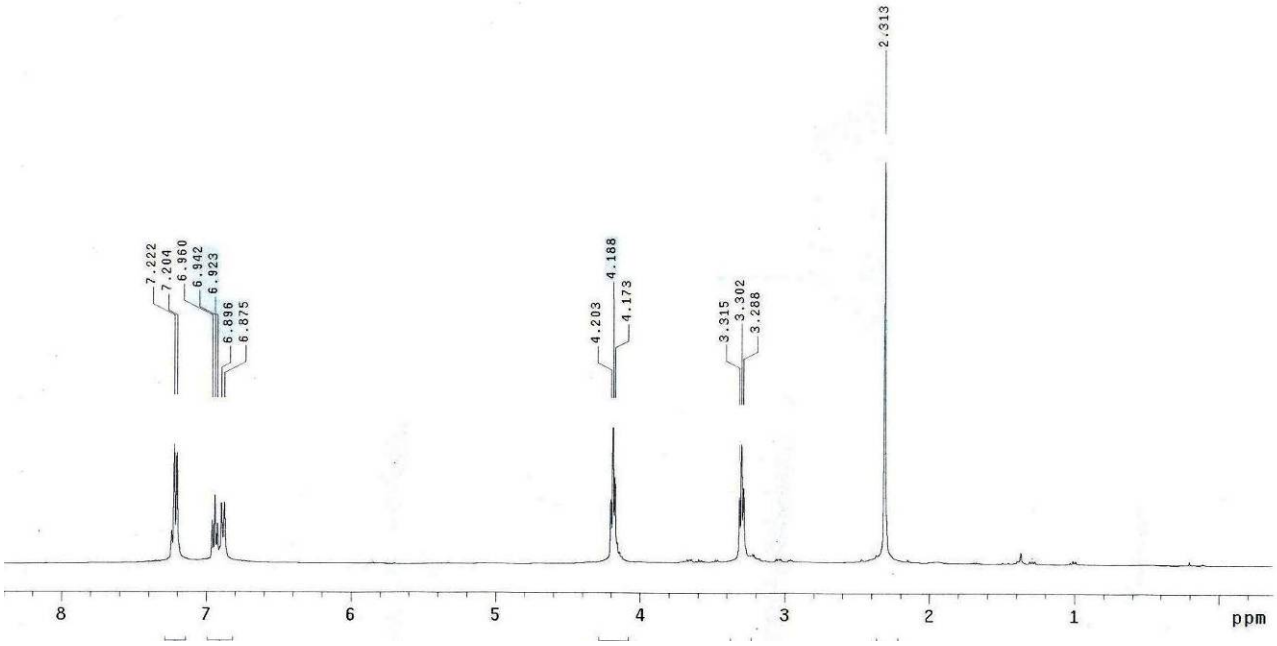

Figure S7. ^{1}H-NMR spectrum of podand **L$_3$** in $CDCl_3$.

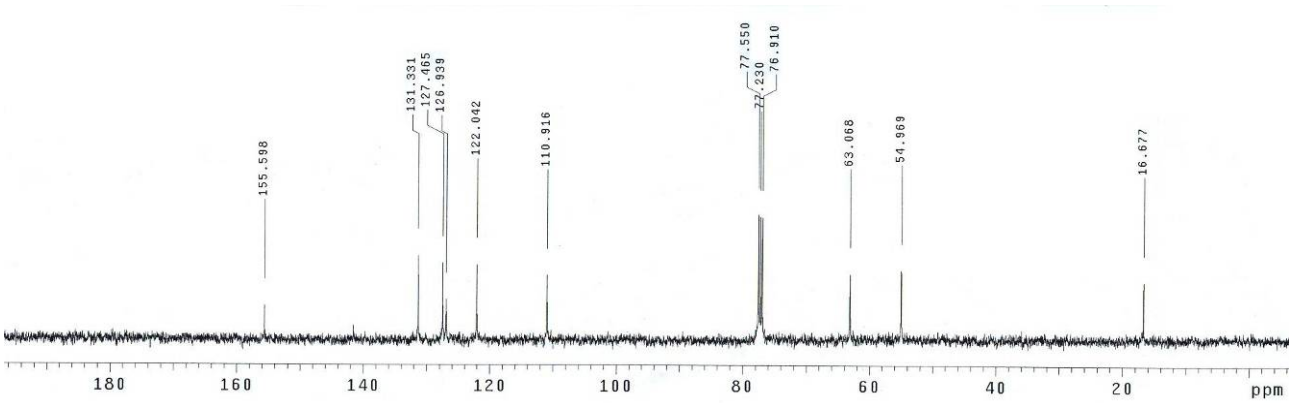

Figure S8. ^{13}C-NMR spectrum of podand **L$_3$** in $CDCl_3$.

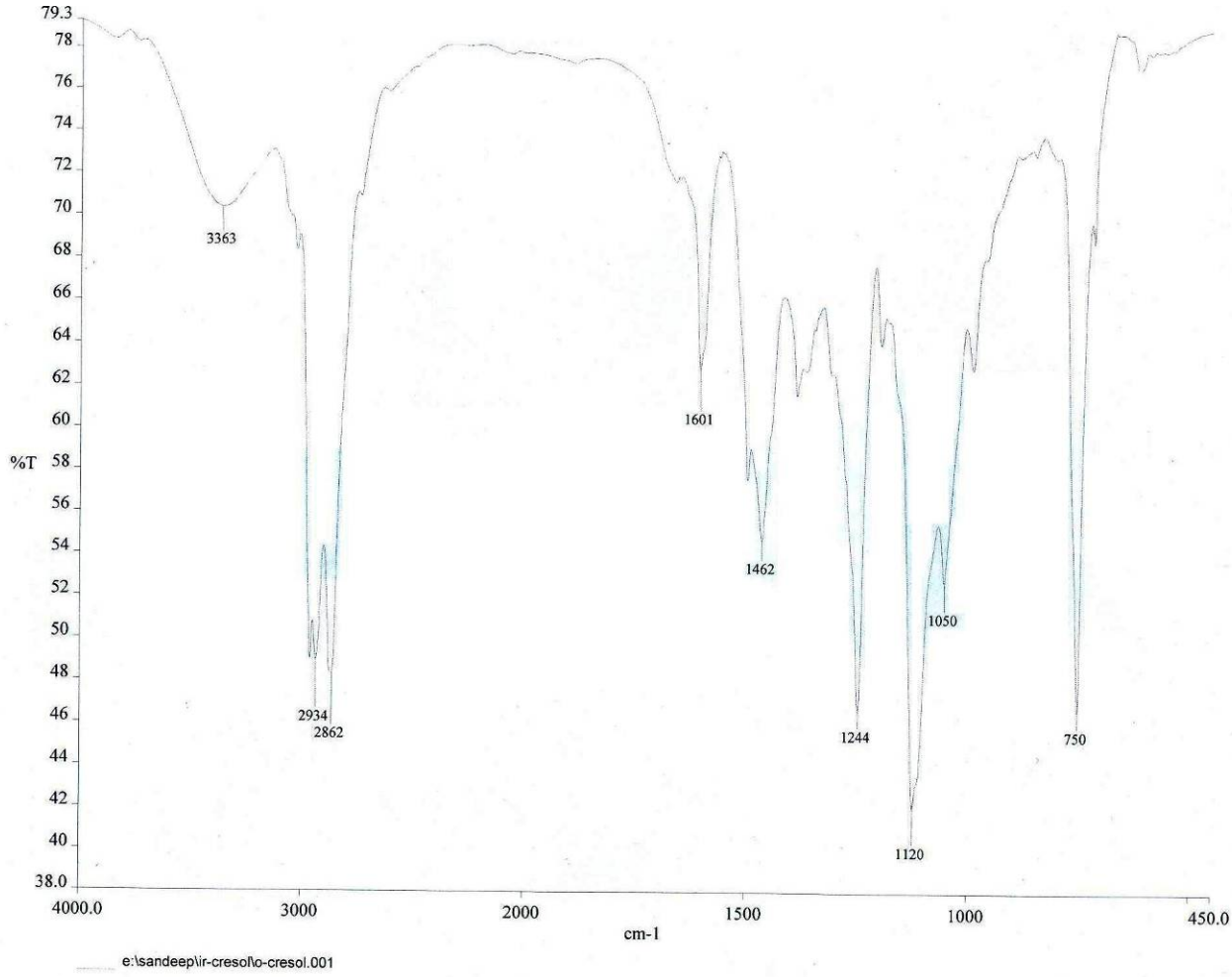

Figure S9. FT-IR spectrum of podand $\mathbf{L_3}$ (KBr pellet).

Characterization of Anion complexes (1-7).

[$H\mathbf{L_1}^+ \bullet ClO_4^-$] **(1).** White crystalline solid; Yield: 94%; ^{1}H-NMR (400 MHz, DMSO-d_6): δ = 2.24 (s, 9H, CH_3), 3.78 (s, 6H, NCH_2), 4.36-4.38 (t, 6H, OCH_2), 6.84-6.86 (d, 6H, ArH), 7.10-7.12 (d, 6H, ArH); IR (KBr disk) ν (cm^{-1}); 1086 (Cl-O), 1241 (C-O).

[$H\mathbf{L_2}^+ \bullet ClO_4^-$] **(2).** White crystalline solid; Yield: 90%; ^{1}H-NMR (400 MHz, DMSO-d_6): δ = 2.16 (s, 9H, CH_3), 3.97 (t, 6H, NCH_2), 4.31-4.33 (t, 6H, OCH_2), 6.35 (s, 3H, ArH), 6.48-6.50 (d, 3H, ArH), 6.76-6.78 (d, 3H, ArH), 7.06-7.10 (t, 3H, ArH); IR (KBr disk) ν (cm^{-1}); 1088 (Cl-O), 1262 (C-O).

[$H\mathbf{L_3}^+ \bullet ClO_4^-$] **(3).** Off white crystalline solid; Yield: 92%; ^{1}H-NMR (400 MHz, DMSO-d_6): δ = 2.11 (s, 9H, CH_3), 3.91-3.94 (t, 6H, NCH_2), 4.43-4.45 (t, 6H, OCH_2), 6.87-6.90 (t, 3H, ArH), 6.94-6.96 (d, 3H, ArH), 7.13-7.18 (m, 6H, ArH); IR (KBr disk) ν (cm^{-1}); 1089 (Cl-O), 1241 (C-O).

[H$\mathbf{L_1}^+$•Br^-]•$2H_2O$ **(4).** White crystalline solid; Yield: 68%; ^{1}H-NMR (400 MHz, DMSO-d_6): δ = 2.22 (s, 9H, CH_3), 3.72-3.75 (t, 6H, NCH_2), 4.38-4.40 (t, 6H, OCH_2), 6.82-6.84 (d, 6H, ArH), 7.07-7.09 (d, 6H, ArH); IR (KBr disk) ν (cm^{-1}); 1272 (C-O).

[H$\mathbf{L_1}^+$•Picrate] **(5)**. Yellow crystalline solid; Yield: 75%; ^{1}H-NMR (400 MHz, DMSO-d_6): δ = 2.22 (s, 9H, CH_3), 3.78 (s, 6H, NCH_2), 4.35-4.38 (t, 6H, OCH_2), 6.82-6.84 (d, 6H, ArH), 7.08-7.10 (d, 6H, ArH), 8.58 (s, 2H, Picrate-H); IR (KBr disk) ν (cm^{-1}); 1233 (C-O).

[H$\mathbf{L_3}^+$•Picrate] **(6)**. Yellow crystalline solid; Yield: 70%; ^{1}H-NMR (400 MHz, DMSO-d_6): δ = 2.10 (s, 9H, CH_3), 3.90-3.92 (t, 6H, NCH_2), 4.42-4.44 (t, 6H, OCH_2), 6.86-6.88 (t, 3H, ArH), 6.93-6.95 (d, 3H, ArH), 7.11-7.15 (m, 6H, ArH), 8.55 (s, 2H, Picrate-H); IR (KBr disk) ν (cm^{-1}); 1238 (C-O).

[H$\mathbf{L_1}^+$•Pyromellitate] **(7)**. White crystalline solid; Yield: 72%; ^{1}H-NMR (400 MHz, DMSO-d_6): δ = 2.20 (s, 9H, CH_3), 3.49 (s, 6H, NCH_2), 4.21-4.23 (t, 6H, OCH_2), 6.79-6.81 (d, 6H, ArH), 7.05-7.07 (d, 6H, ArH), 8.28 (s, 2H, PMA-H); IR (KBr disk) ν (cm^{-1}); 1251 (C-O).

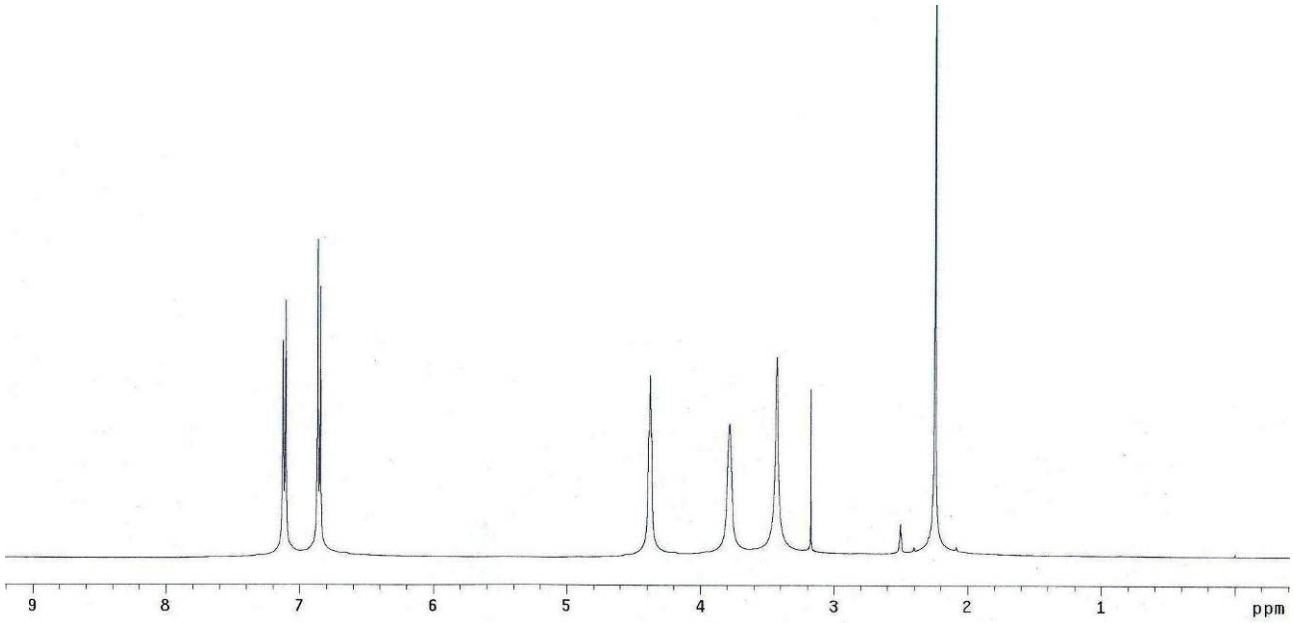

Figure S10. ^{1}H-NMR spectrum of [H$\mathbf{L_1}^+$•ClO_4^-] **(1)** in DMSO-d_6.

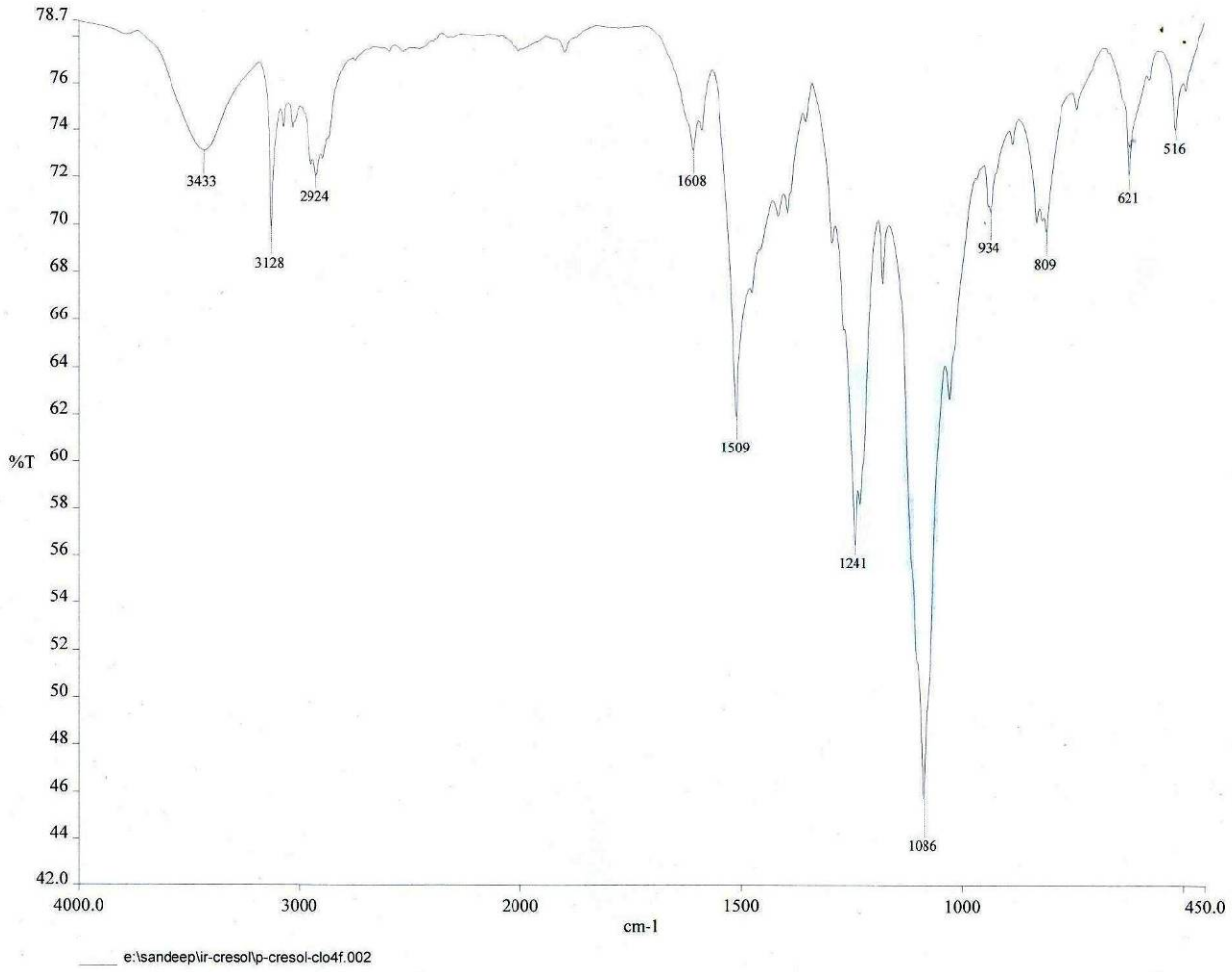

Figure S11. FT-IR spectrum of [H$\mathbf{L_1}^+$•ClO_4^-] **(1)** (KBr pellet).

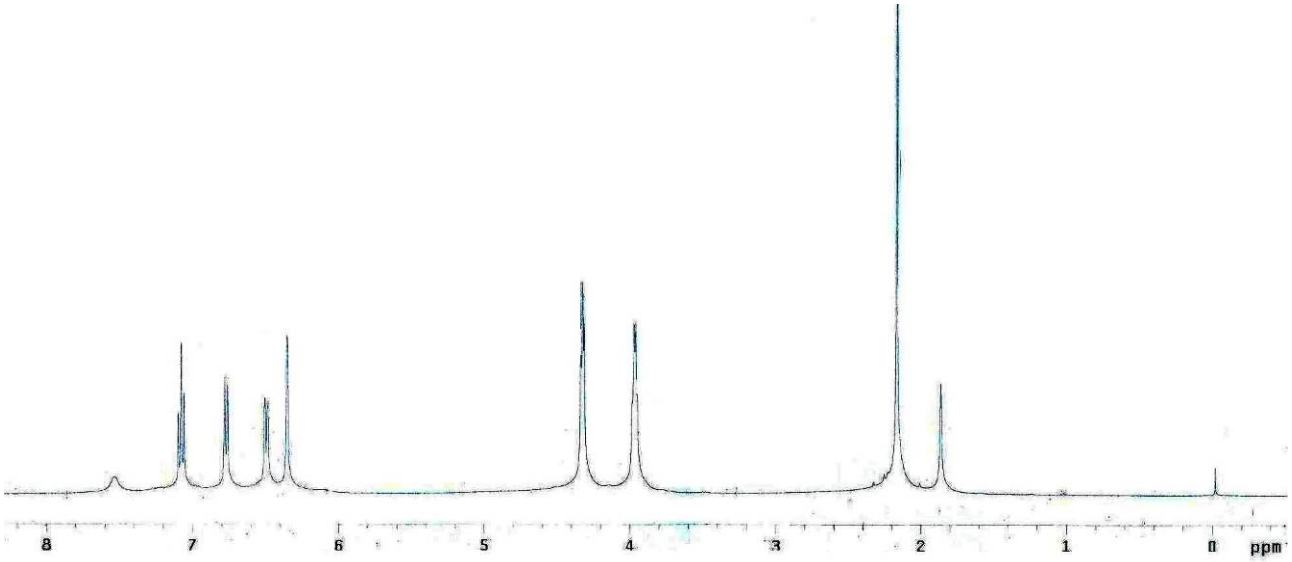

Figure S12. ^{1}H-NMR spectrum of [H$\mathbf{L_2}^+$•ClO_4^-] **(2)** in DMSO-d_6.

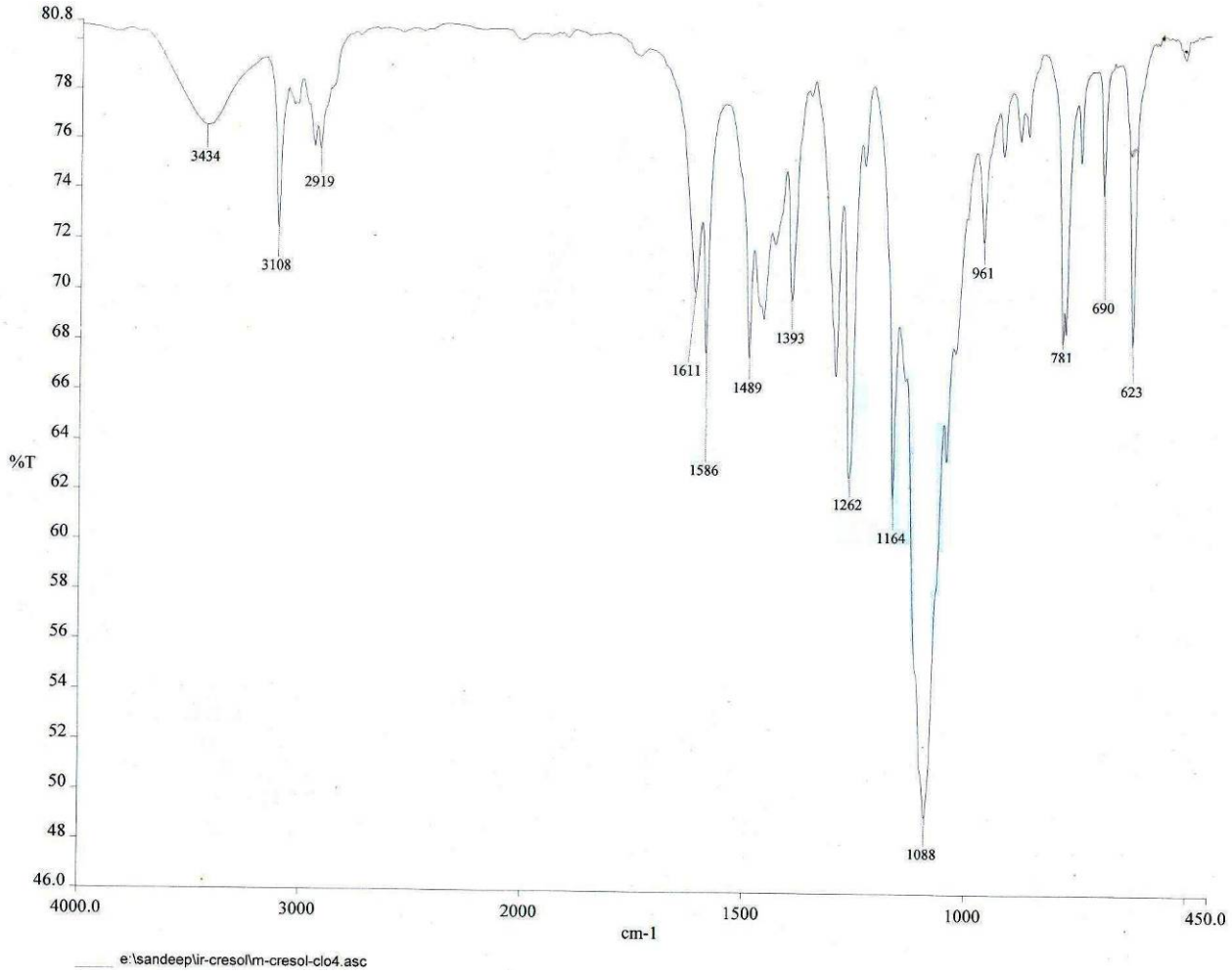

Figure S13. FT-IR spectrum of [H**L₂**$^+$•ClO_4^-] **(2)** (KBr pellet).

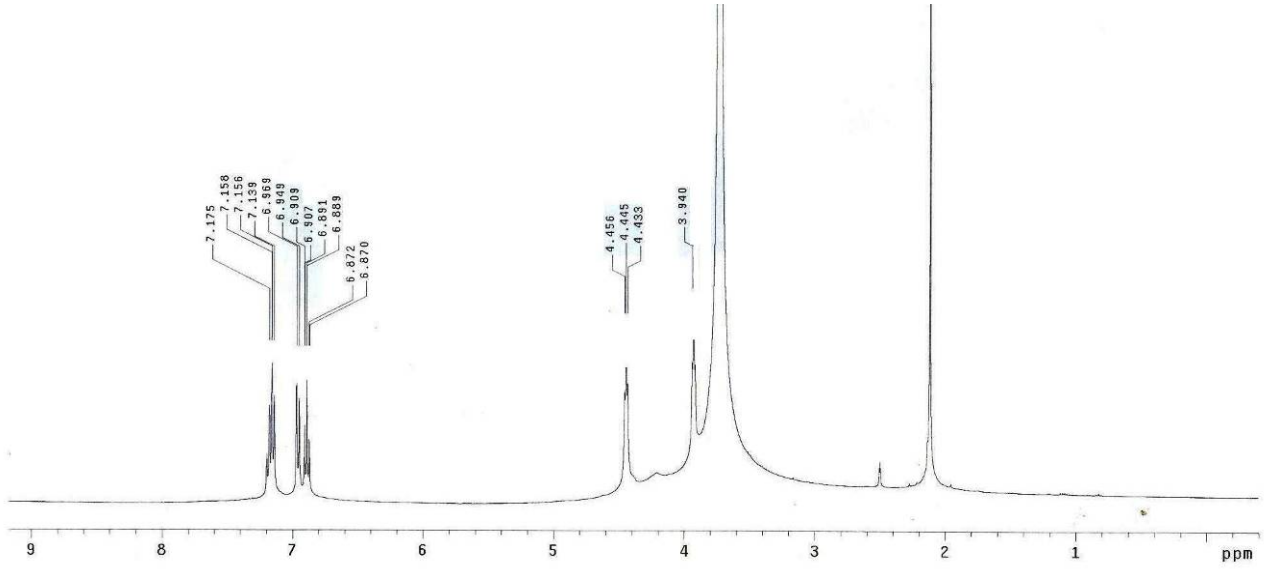

Figure S14. ^{1}H-NMR spectrum of [H**L₃**$^+$•ClO_4^-] **(3)** in DMSO-d_6.

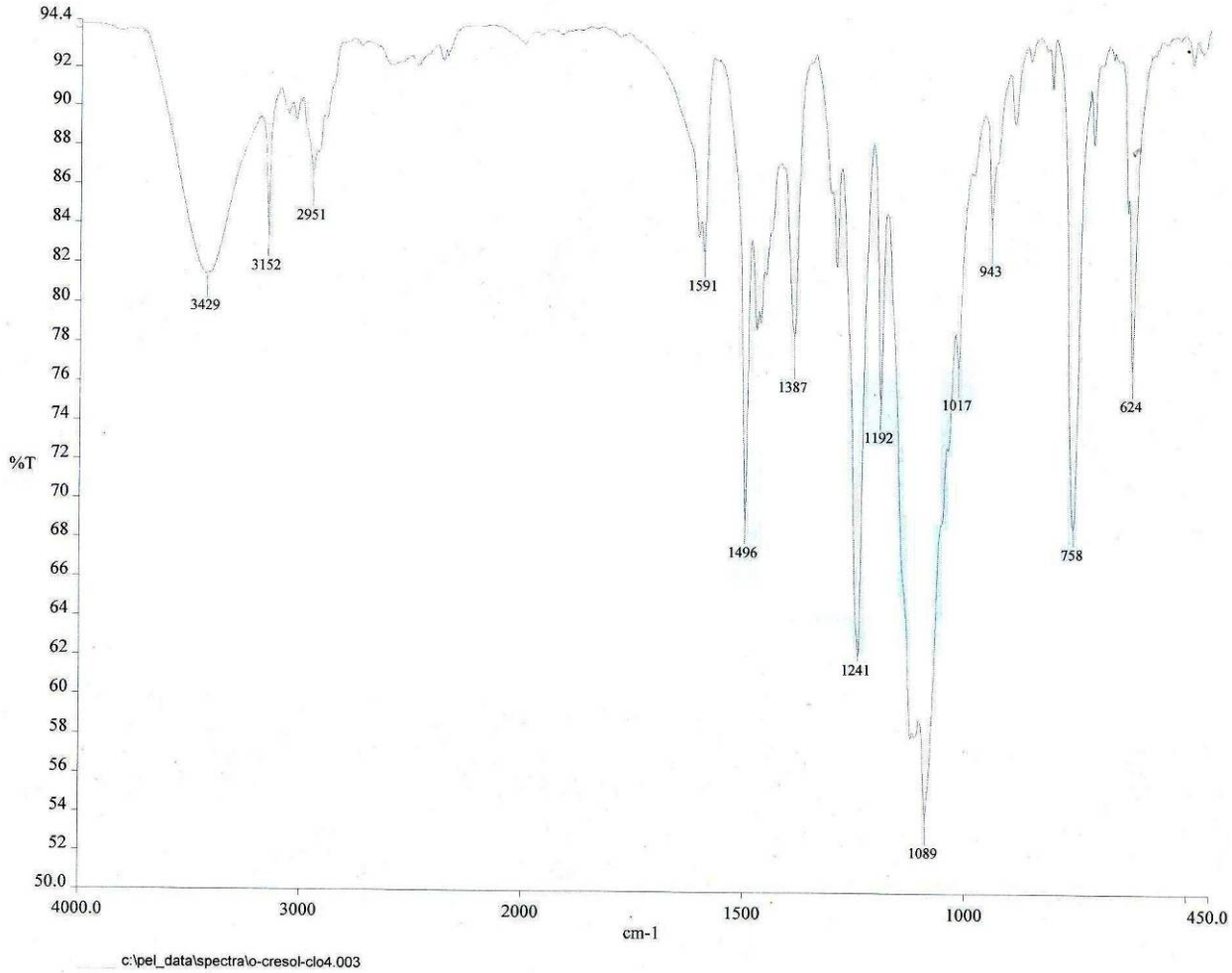

Figure S15. FT-IR spectrum of [H$\mathbf{L_3}^+$•ClO_4^-] **(3)** (KBr pellet).

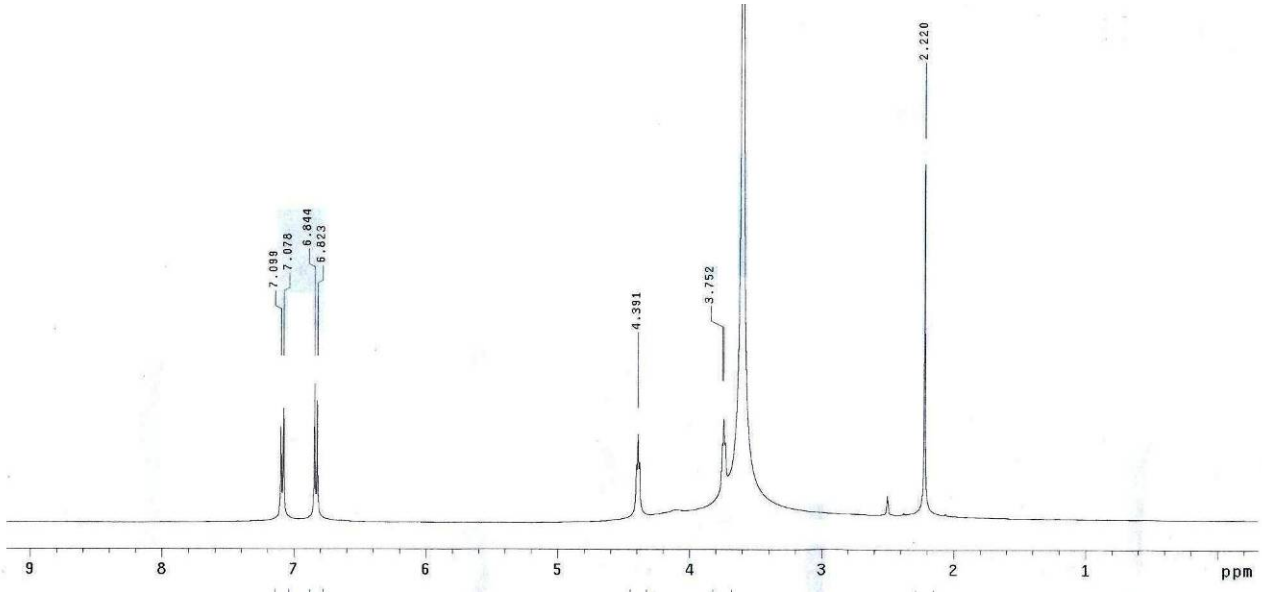

Figure S16. ^{1}H-NMR spectrum of complex [H$\mathbf{L_1}^+$•Br^-]•$2H_2O$ **(4)** in DMSO-d_6.

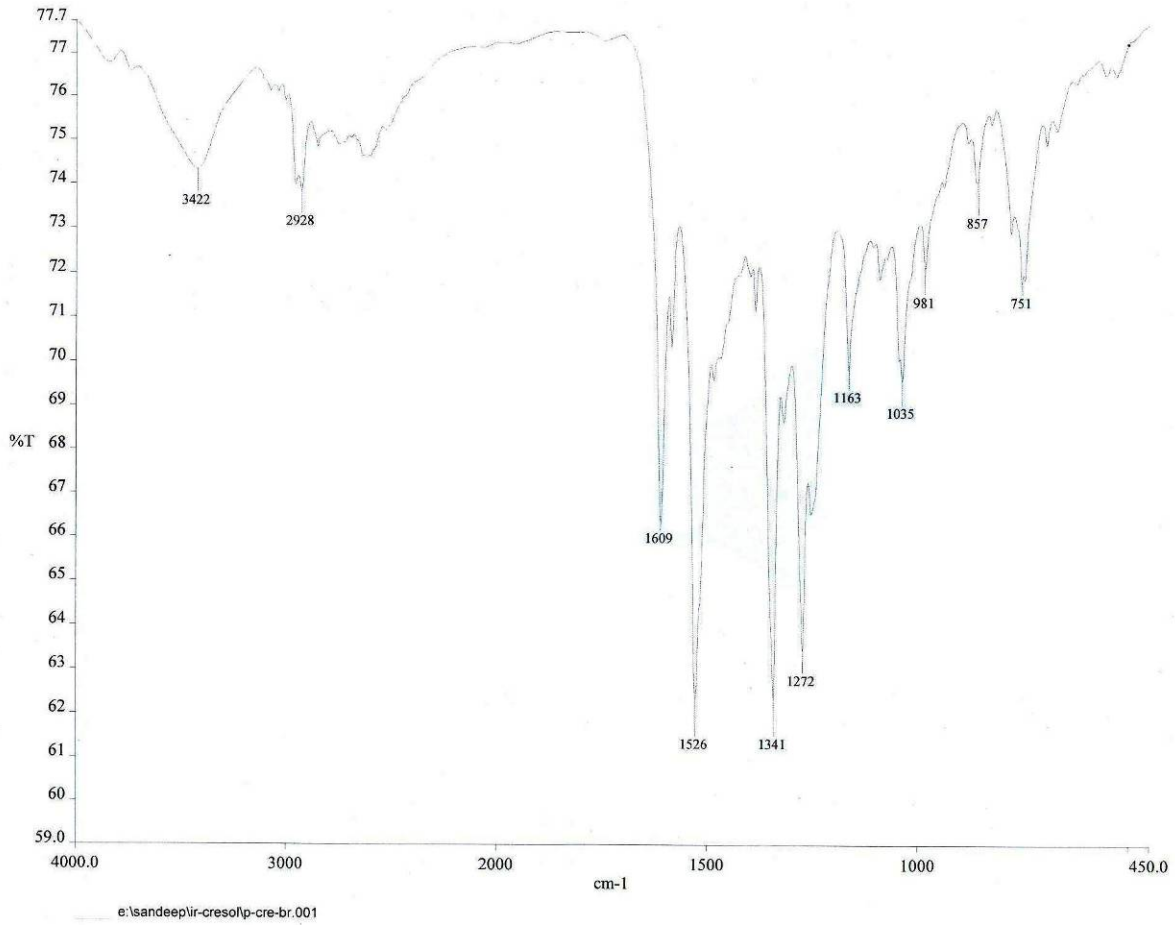

Figure S17. FT-IR spectrum of [H$\mathbf{L_1}^+$•Br^-]•$2H_2O$ **(4)** (KBr pellet).

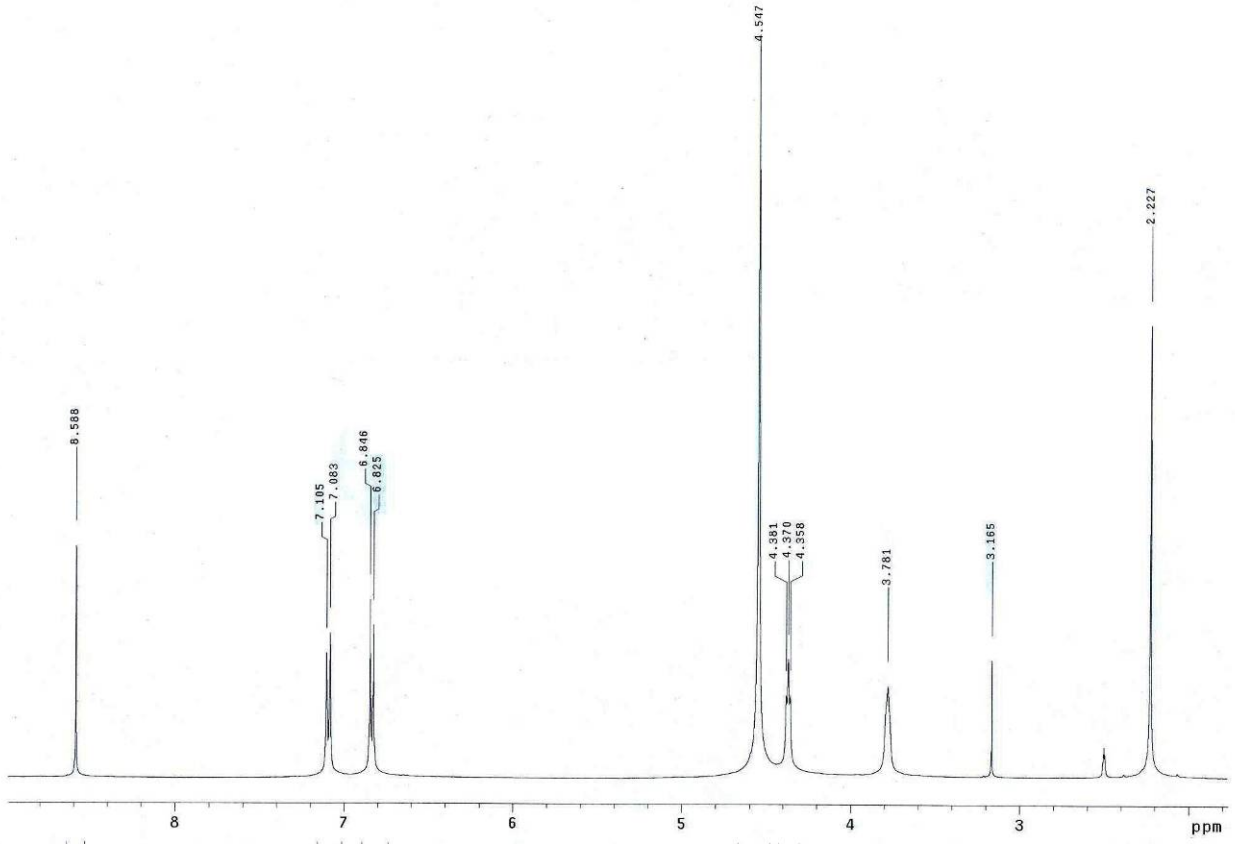

Figure S18. ^{1}H-NMR spectrum of [H$\mathbf{L_1}^+$•Picrate] **(5)** in DMSO-d_6.

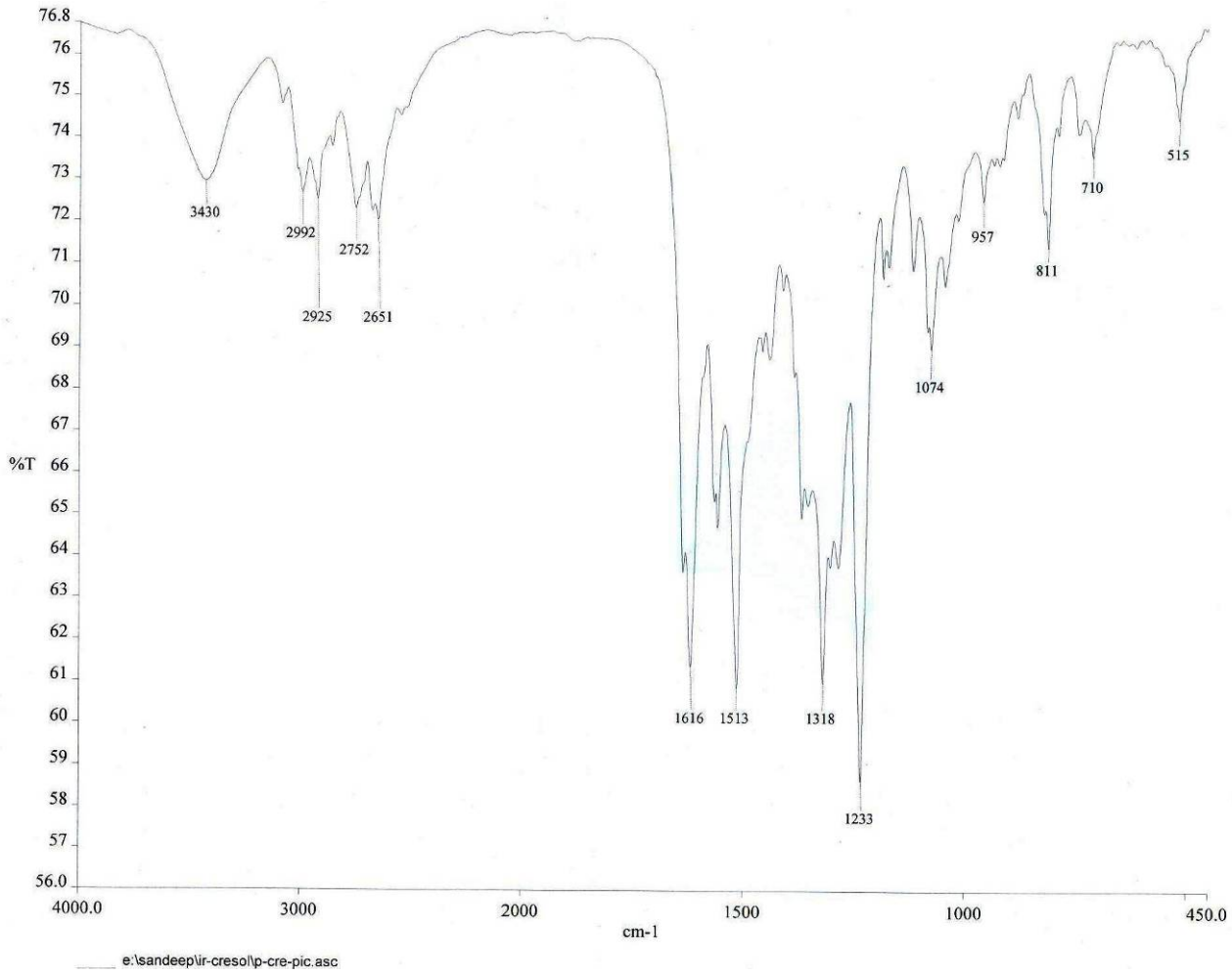

Figure S19. FT-IR spectrum of [H$\mathbf{L_1}^+$•Picrate] **(5)** (KBr pellet).

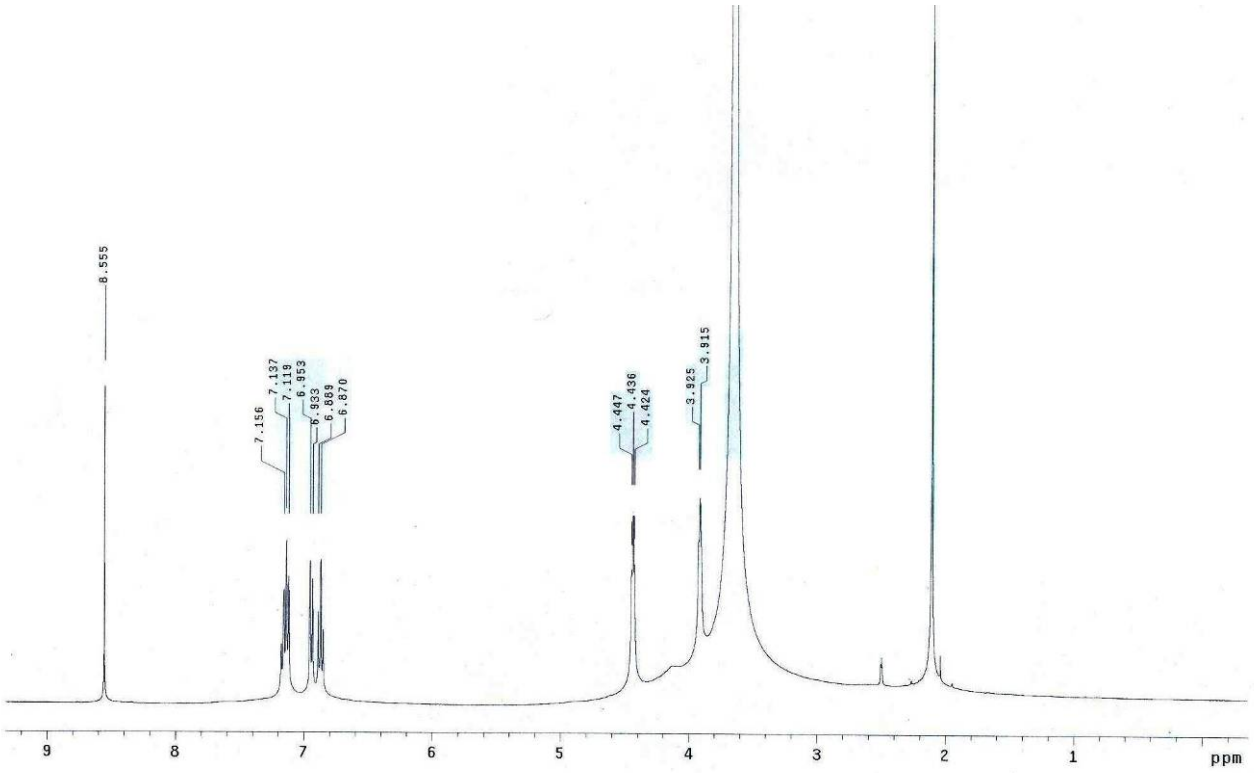

Figure S20. ^{1}H-NMR spectrum of [H$\mathbf{L_3}^+$•Picrate] **(6)** in DMSO-d_6.

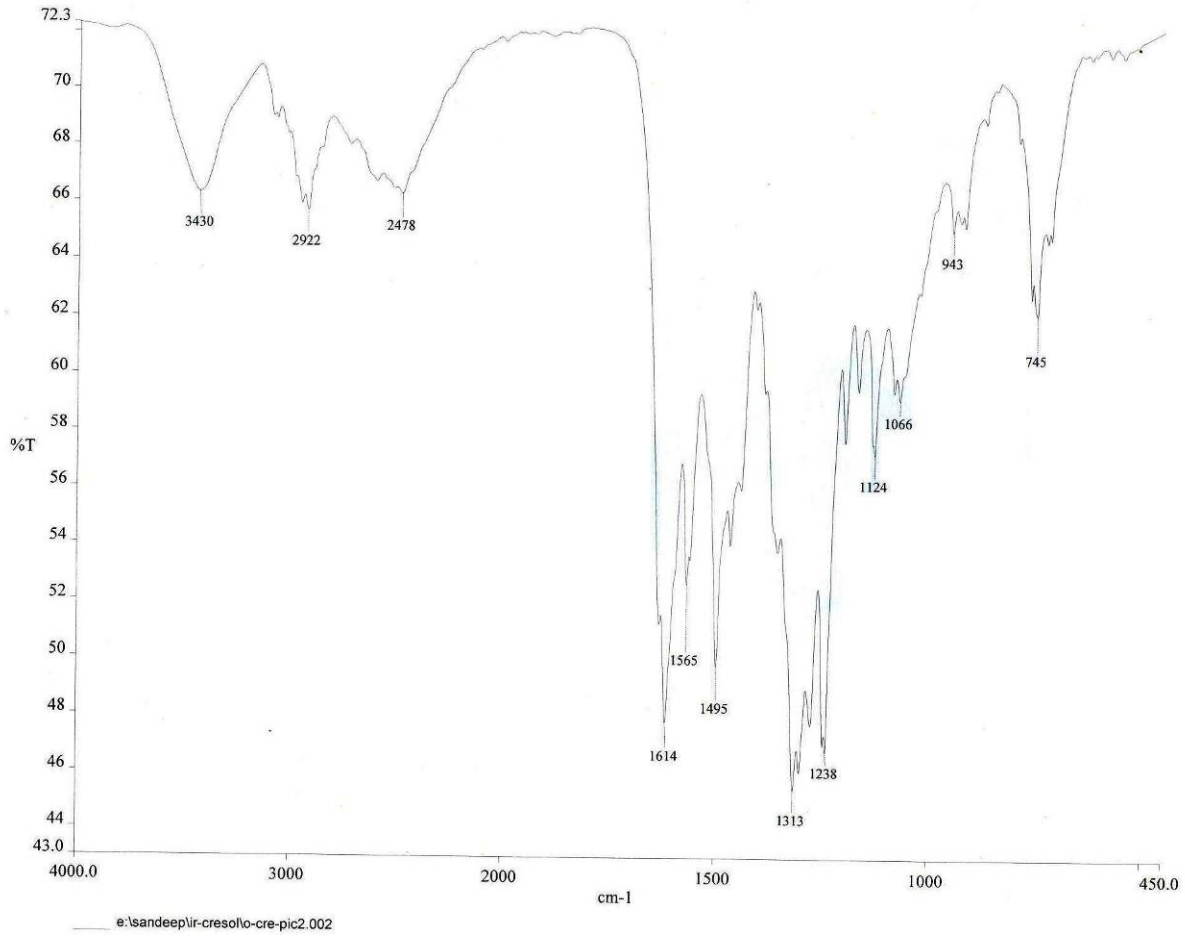

Figure S21. FT-IR spectrum of [H$\mathbf{L_3}^+$•Picrate] **(6)** (KBr pellet).

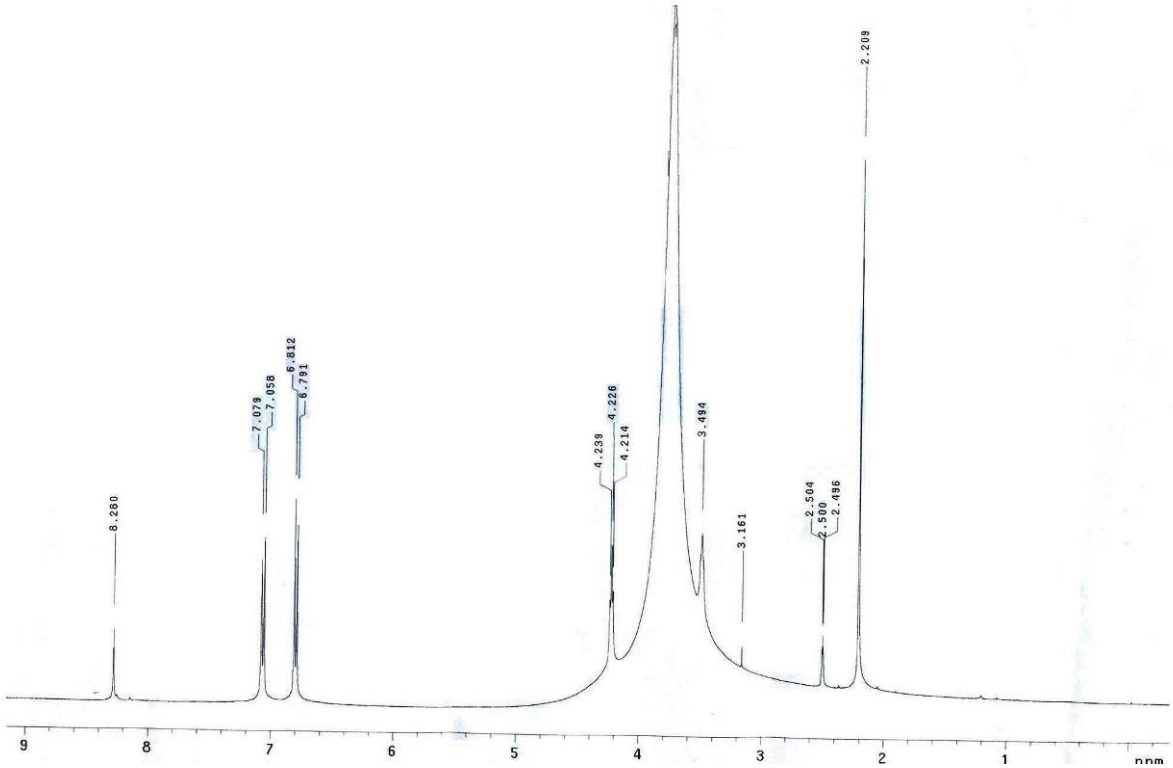

Figure S22. ^{1}H-NMR spectrum of [H$\mathbf{L_3}^+$•Pyromellitate] **(7)** in DMSO-d_6.

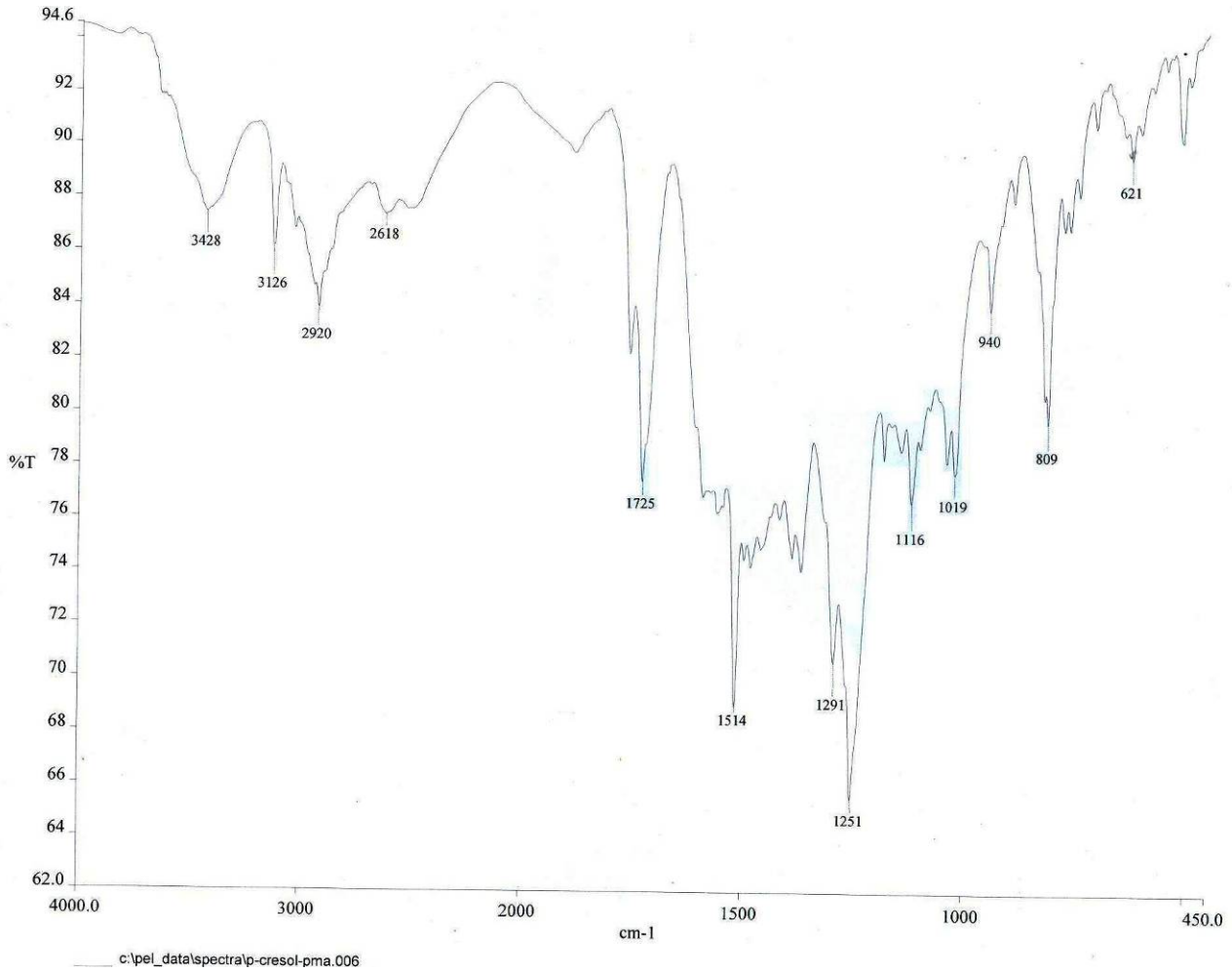

Figure S23. FT-IR spectrum of [H$\mathbf{L_3}^+$•Pyromellitate] **(7)** (KBr pellet).

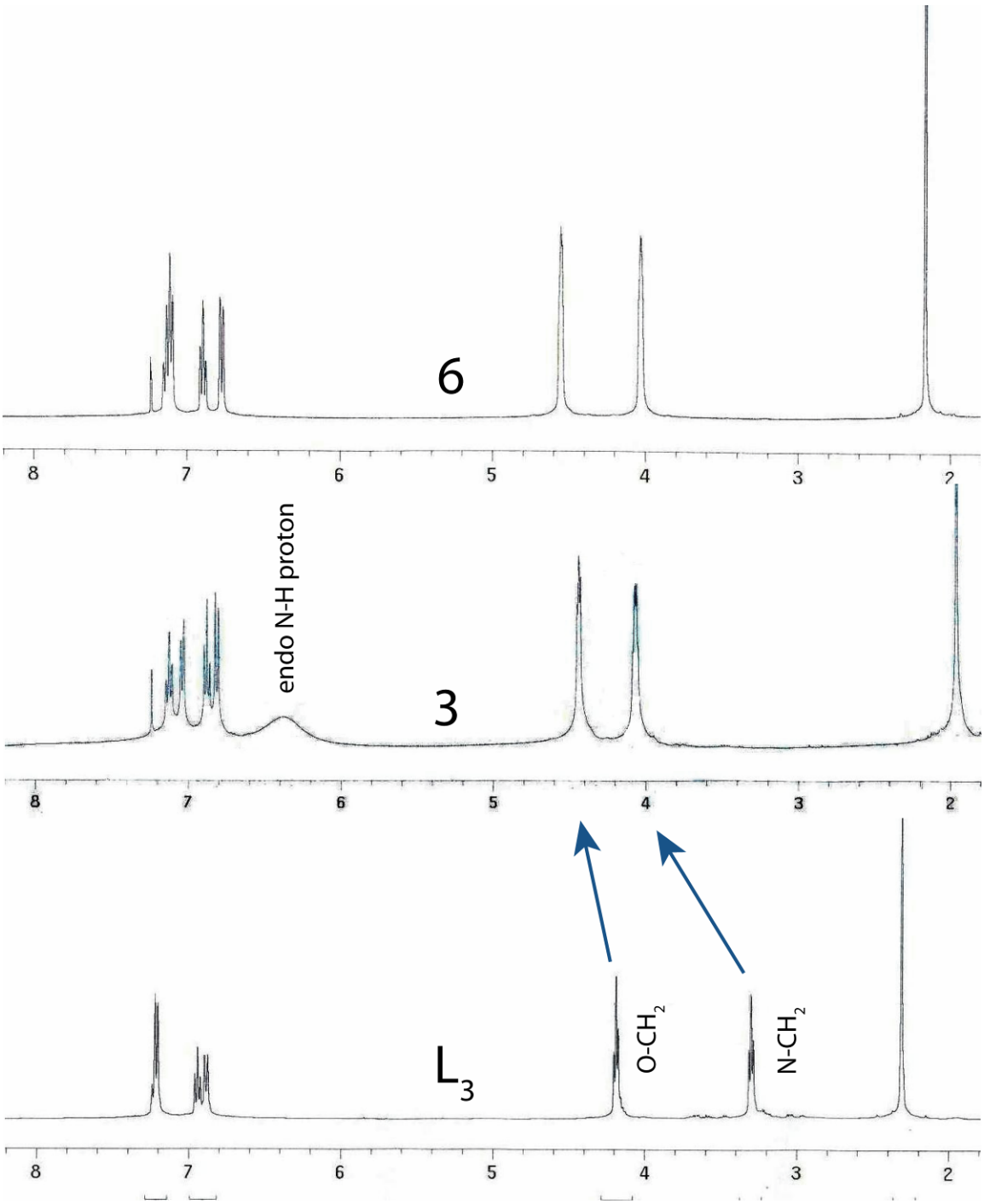

Figure S24. Comparison of the ^{1}H NMR spectra ($CDCl_3$) of complexes **3** and **6** with $\mathbf{L_3}$ demonstrating the occurrence of apical N-H proton resonances at δ = 6.392 ppm for **3** whereas no N-H proton resonances has been observed for **6**.

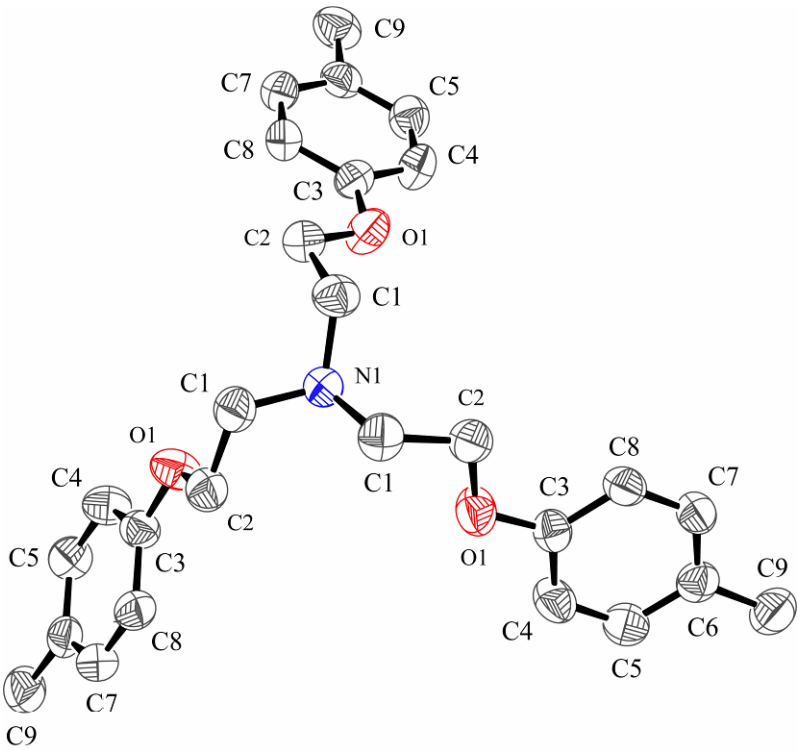

Figure S25. ORTEP plot (50% probability ellipsoids) of tripodal podand $\mathbf{L_1}$.

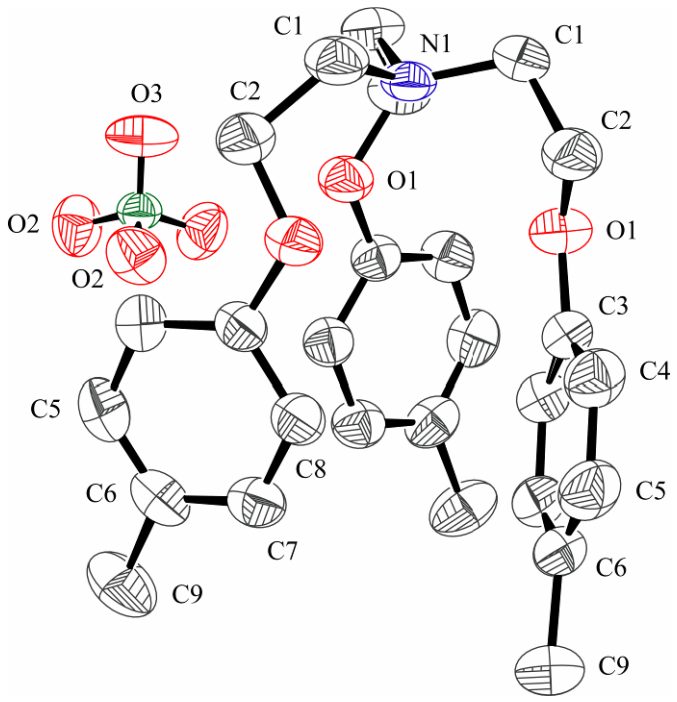

Figure S26. ORTEP plot (50% probability ellipsoids) of **1**.

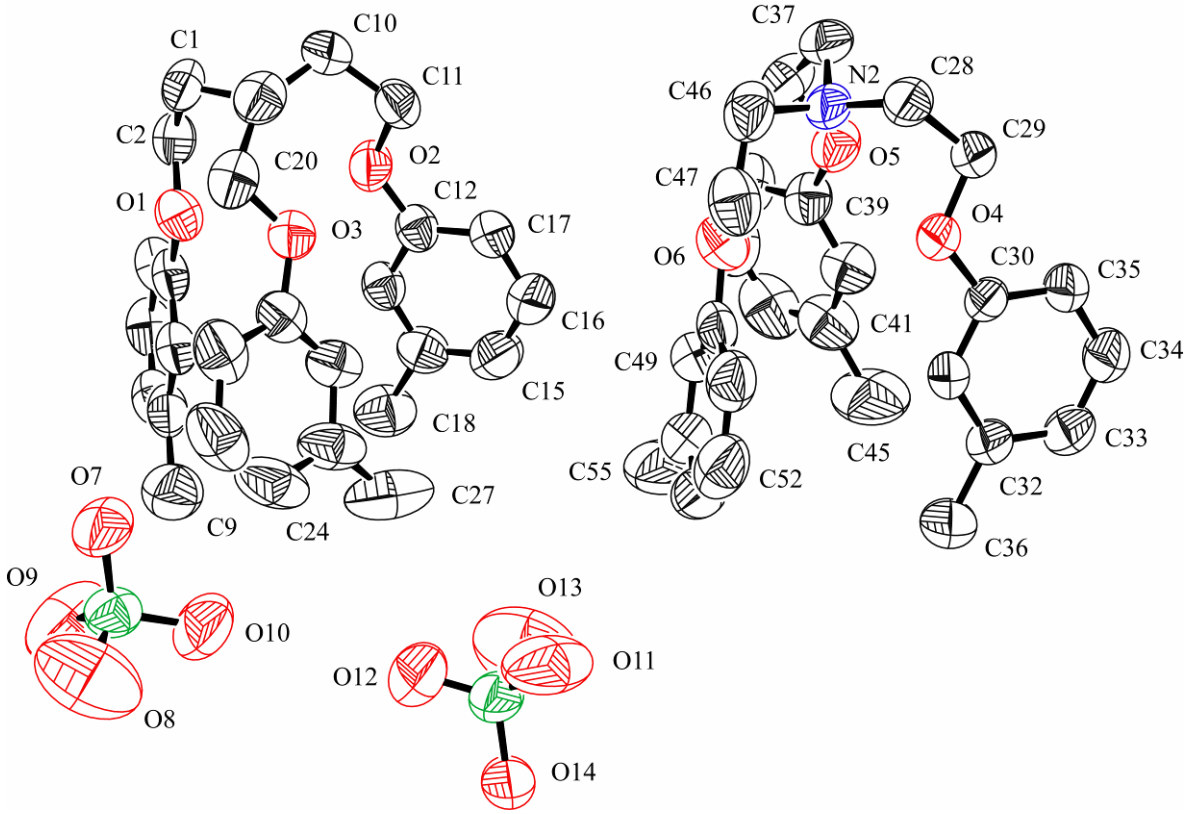

Figure S27. ORTEP plot (50% probability ellipsoids) of **2**.

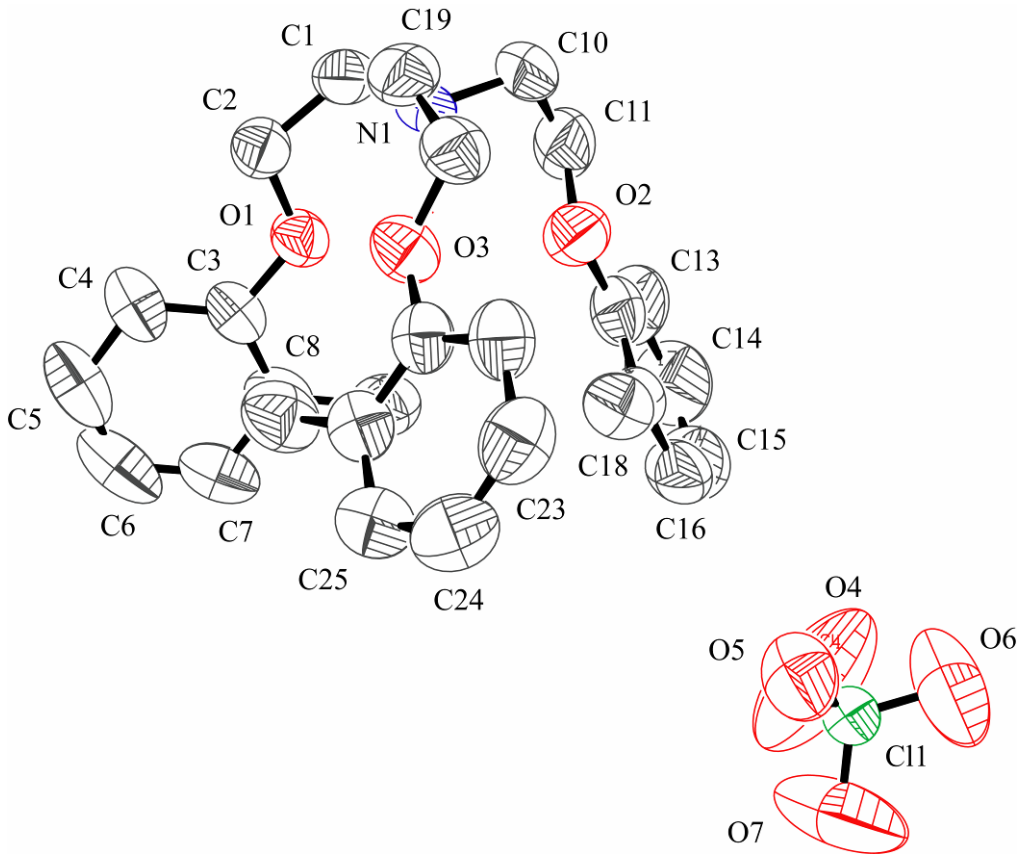

Figure S28. ORTEP plot (50% probability ellipsoids) of **3**.

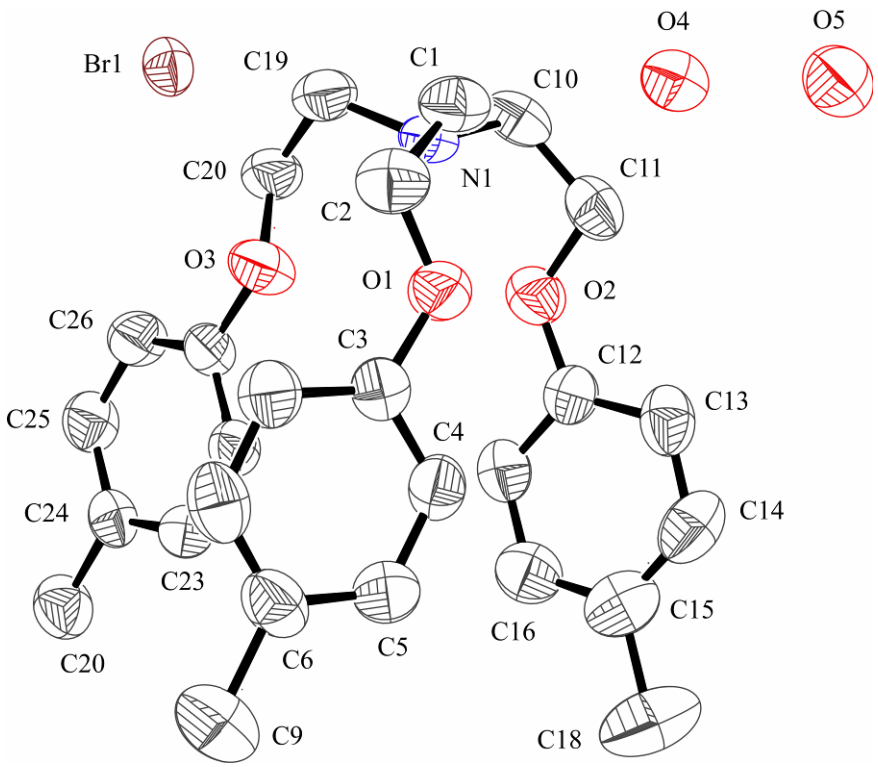

Figure S29. ORTEP plot (50% probability ellipsoids) of **4**.

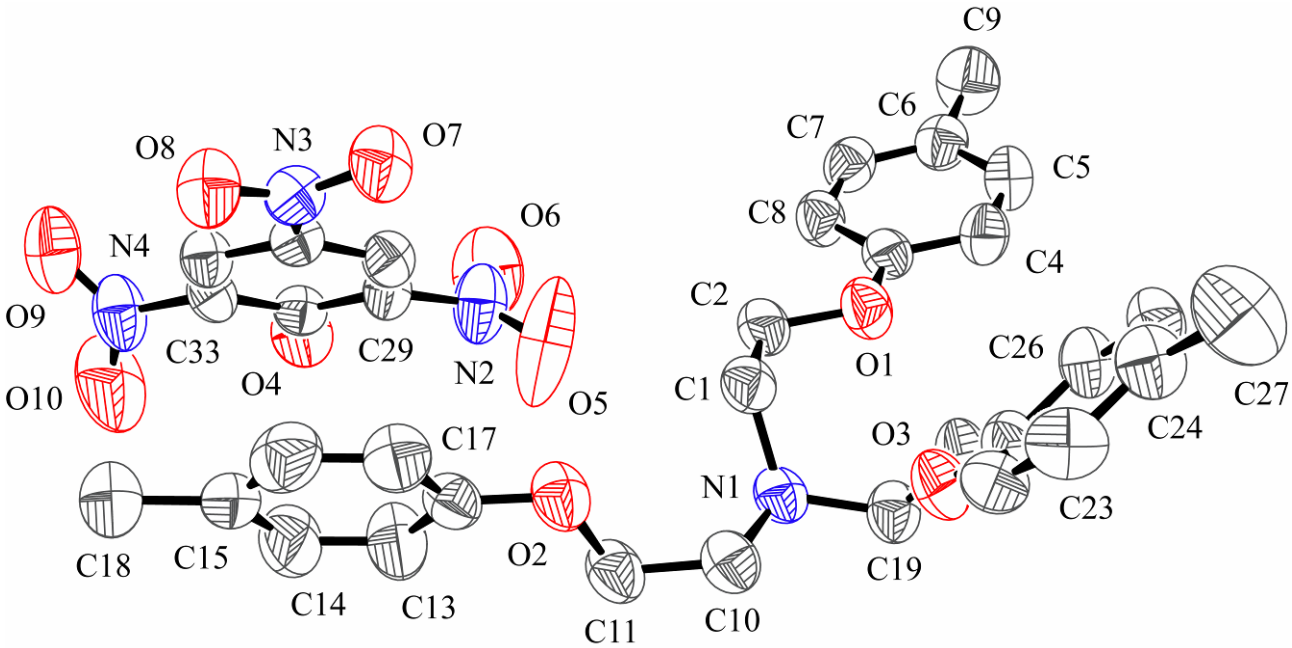

Figure S30. ORTEP plot (50% probability ellipsoids) of **5**.

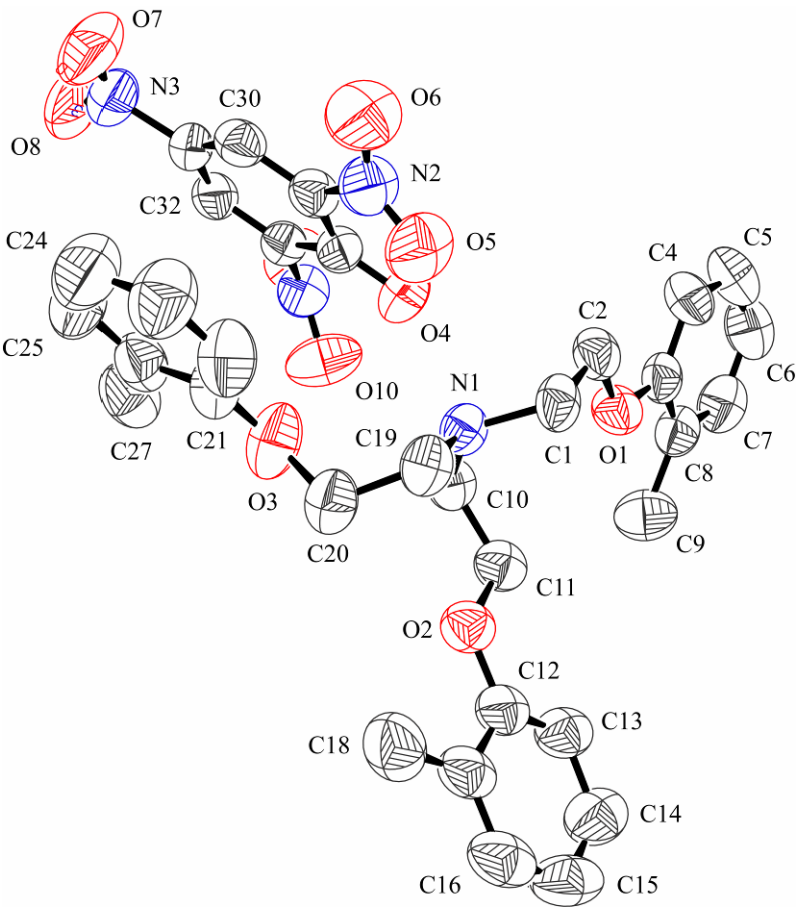

Figure S31. ORTEP plot (50% probability ellipsoids) of **6**.

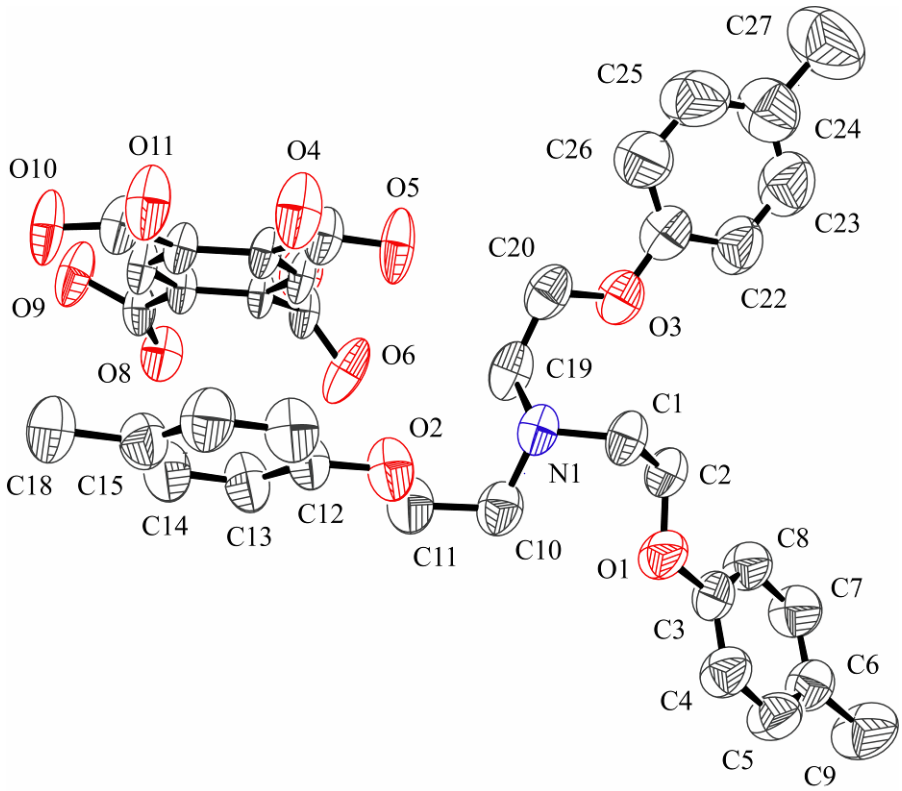

Figure S32. ORTEP plot (50% probability ellipsoids) of **7**.

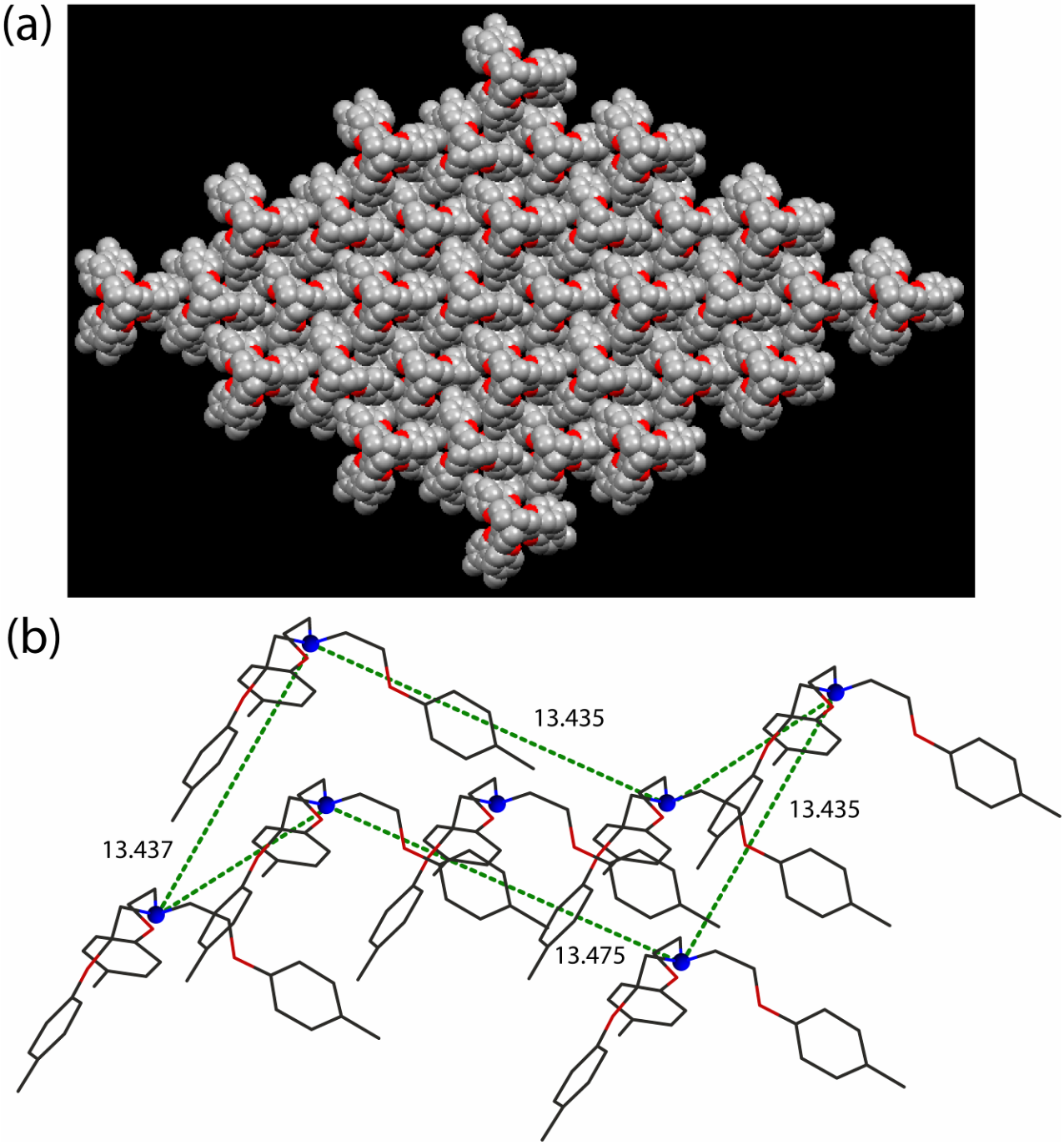

Figure S33. (a) Spacefill model of crystal packing in $\mathbf{L_1}$ viewed down the crystallographic *c* axis depicting the formation of honey comb like structure; (b) Crystal structure of $\mathbf{L_1}$, showing hexagonal arrangement of tripodal unit around each central ligand forming chair-form of cyclohexane conformation (N_{apical} •••• N_{apical} = 13.475 Å).

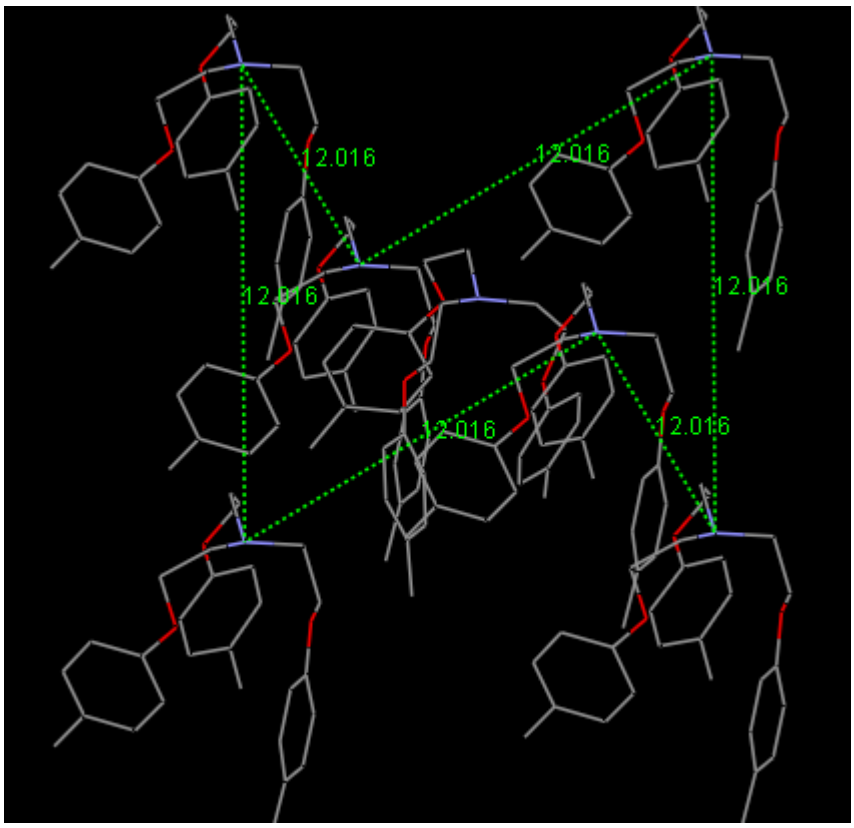

Figure S34. Crystal structure of **1**, showing hexagonal arrangement of tripodal unit around each central ligand forming chair-form of cyclohexane conformation (N_{apical} •••• N_{apical} = 13.475 Å).

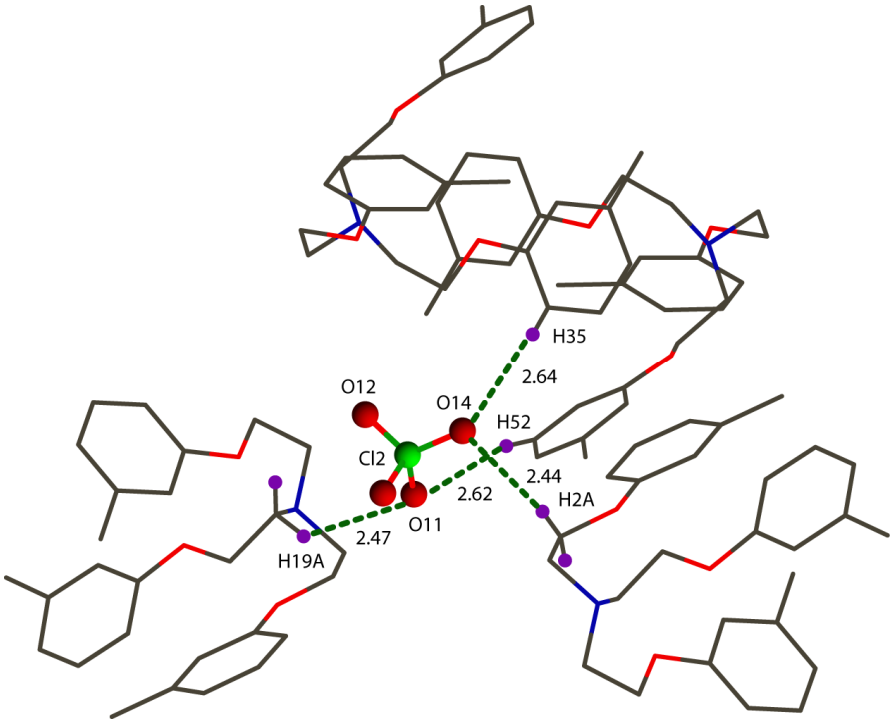

Figure S35. Close-up view of the C-H hydrogen bonding contacts on $Cl(2)O_4^-$ anion in **2** (green dotted lines) with four encircling $\mathbf{L_2}H^+$ units with relevant H-bond distances.

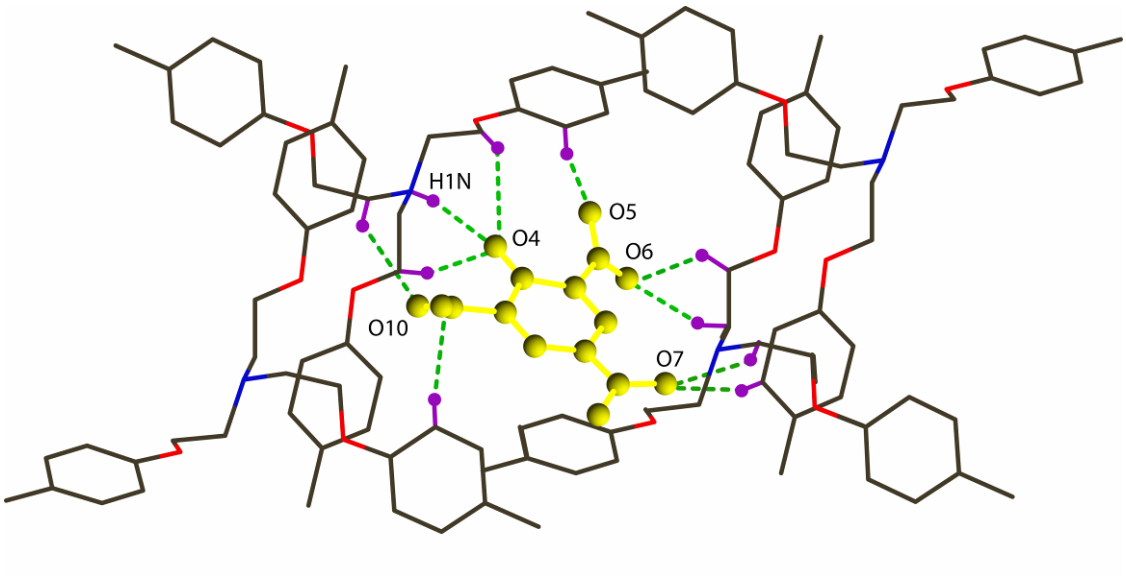

Figure S36. (a) Close-up view of the nine C-H···O hydrogen-bonding interactions of picrate anion (green dotted lines) with various aliphatic and aromatic hydrogen atoms of the five encircling cationic units in complex **5**. Picrate anion has been shown in yellow and the interacting H-atoms are depicted in purple colour for the clarity of presentation.

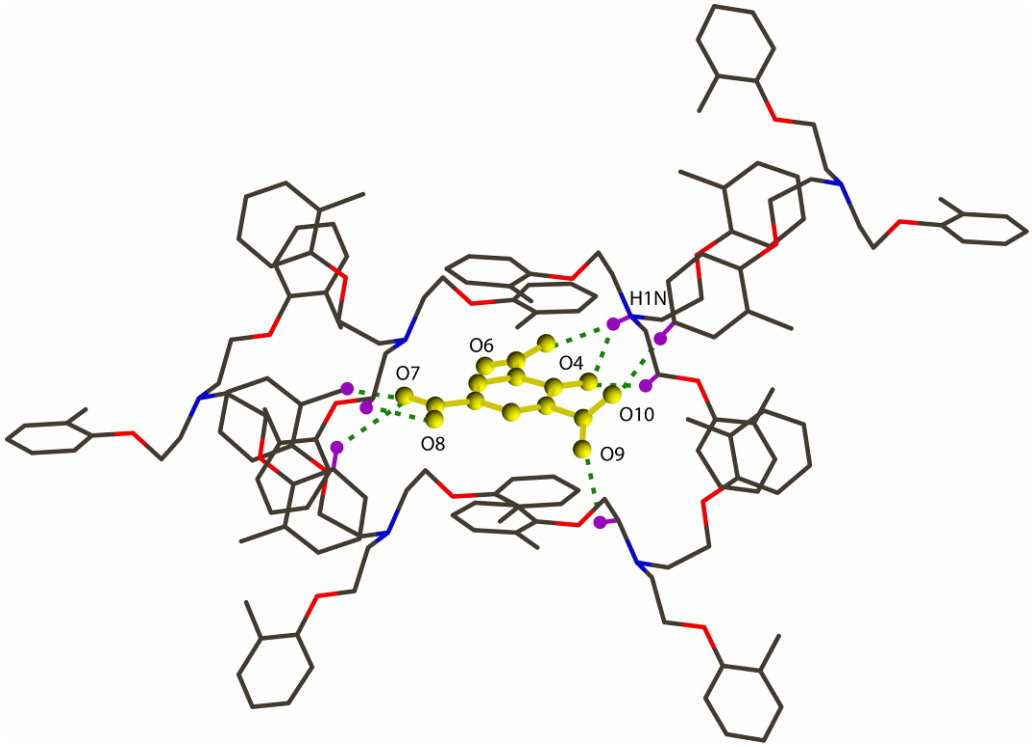

Figure S37. (a) Close-up view of the six C-H···O hydrogen-bonding interactions of picrate anion (green dotted lines) with various aliphatic and aromatic hydrogen atoms of the six encircling cationic units in complex **6**. Picrate anion has been shown in yellow and the interacting H-atoms are depicted in purple colour for the clarity of presentation.

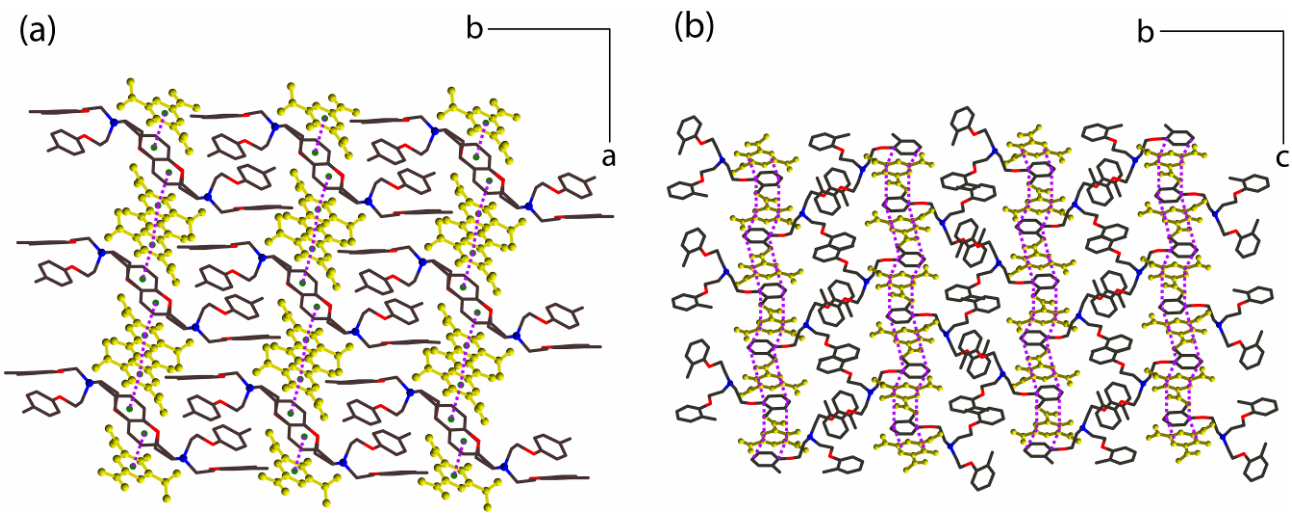

Figure S38. Crystal packing diagram of complexes **5** (a) and **6** (b) as viewed down the crystallographic *c*- and *a*-axis, depicting the aromatic π····π stacking interactions between a phenyl ring tripodal cations with the picrate anion along *a*- and *c*-axis respectively.

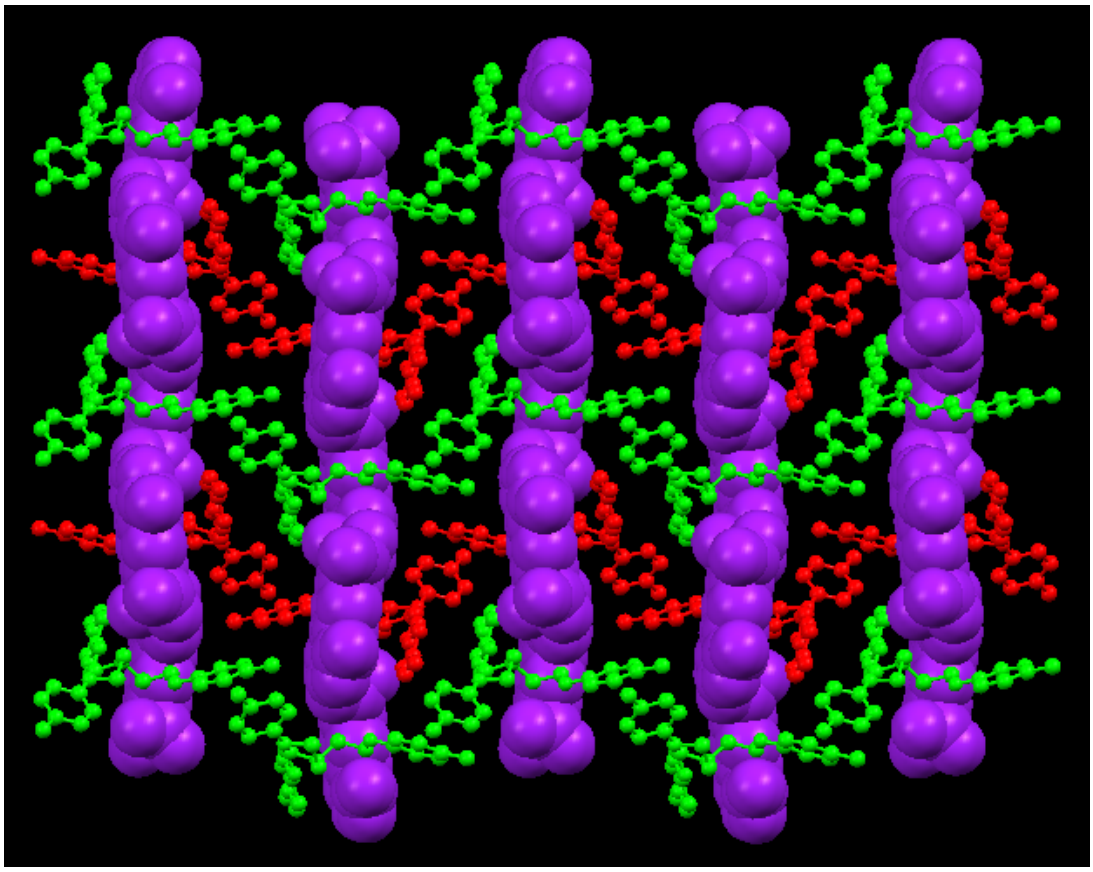

Figure S39. Crystal packing diagram (spacefill representation) of complex **7** as viewed along the crystallographic *a*-axis.

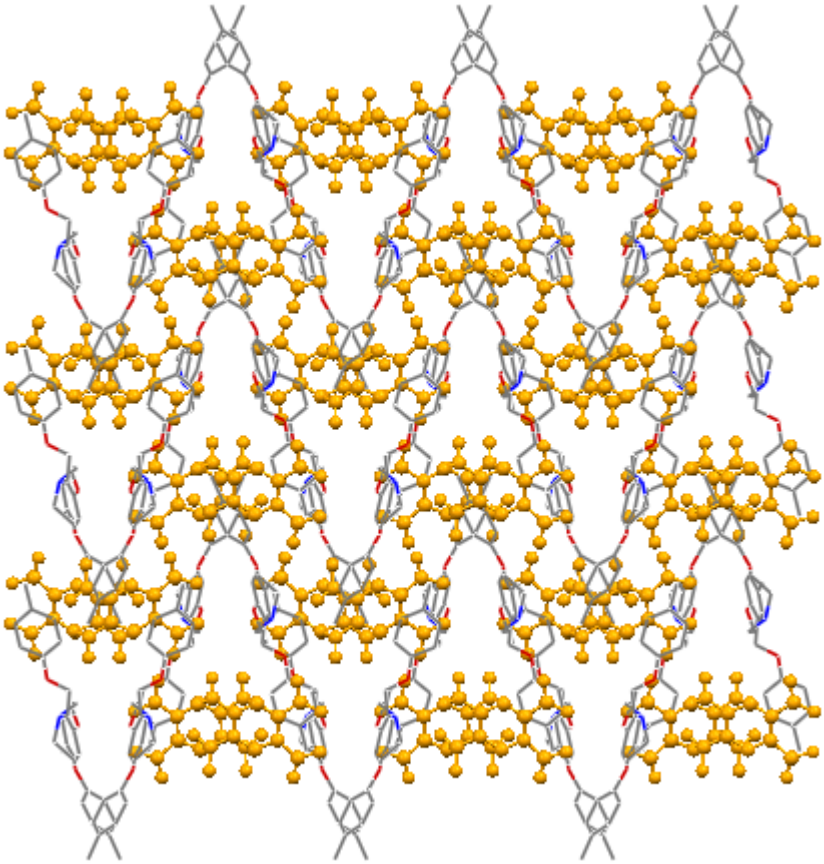

Figure S40. Crystal packing diagram (ball and stick representation) of complex **7** as viewed along the crystallographic *c*-axis.